International Journal of Biological Macromolecules 205 (2022) 638–650

Contents lists available at ScienceDirect

International Journal of Biological Macromolecules

journal homepage: www.elsevier.com/locate/ijbiomac

A dual functional chondro-inductive chitosan thermogel with high shear modulus and sustained drug release for cartilage tissue engineering

Dorsa Dehghan-Baniani [a,b], Babak Mehrjou [c], Dong Wang [d], Reza Bagheri [b], Atefeh Solouk [e], Paul K. Chu [c], Hongkai Wu [a,d,*]

[a] Department of Chemical and Biological Engineering, Division of Biomedical Engineering, The Hong Kong University of Science and Technology, Hong Kong, China
[b] Polymeric Materials Research Group, Department of Materials Science and Engineering, Sharif University of Technology, Tehran, P.O. Box 11155-9466, Iran
[c] Department of Physics, Department of Materials Science and Engineering, Department of Biomedical Engineering, City University of Hong Kong, Tat Chee Avenue, Kowloon, Hong Kong, China
[d] Department of Chemistry, The Hong Kong University of Science and Technology, Hong Kong, China
[e] Department of Biomedical Engineering, Amirkabir University of Technology, Tehran, Iran

ARTICLE INFO

Keywords:
Chitosan hydrogel
Cartilage tissue engineering
Kartogenin
Starch microspheres

ABSTRACT

We report a chitosan-based nanocomposite thermogel with superior shear modulus resembling that of cartilage and dual pro-chondrogenic and anti-inflammatory functions. Two therapeutic agents, kartogenin (KGN) and diclofenac sodium (DS), are employed to promote chondrogenesis of stem cells and suppress inflammation, respectively. To extend the release time in a controlled manner, KGN is encapsulated in the uniform-sized starch microspheres and DS is loaded into the halloysite nanotubes. Both drug carriers are doped into the maleimide-modified chitosan hydrogel to produce a shear modulus of 167 ± 5 kPa that is comparable to that of articular cartilage (50–250 kPa). Owing to the hydrogel injectability and relatively suitable gelation time (5 ± 0.5 min) at 37 °C, this system potentially constitutes a manageable platform for clinical practice. Moreover, sustained linear drug release for over a month boosts chondro-differentiation of stem cells to eliminate the necessity for multiple administrations. Considering virtues such as thermogel strength and ability to co-deliver anti-inflammatory and chondro-inductive biomolecules continuously, the materials and strategy have promising potential in functional cartilage tissue engineering.

1. Introduction

Articular cartilage is a hydrated flexible connective tissue with a complex structure and exceptional load-bearing properties which enable smooth and painless joint movements. However, self-restoration of damaged cartilage is very challenging due to its aneural and avascular nature which is populated with low density of only one cell type that is chondrocytes. Chondrocytes are very specialized mature cell types which deposit ECM with very slow turnover rate. Chondrocytes in articular cartilage have several phenotypes across the cartilage depth, possessing different morphologies, densities and configurations along collagen fibrils leading to spatial variations in ECM composition. They are unstable in terms of phenotypes; once they de-differentiate into fibroblastic or hypertrophic forms, they will deposit a weak defective ECM with poor mechanical properties [1]. Although defective cartilage is not life threatening, the life quality of patients is compromised [2,3]. Moreover, cartilage injuries and related catabolic processes are irreversible leading to osteoarthritis, a common degenerative disease manifested as amplified inflammation and severe pain in the joints [4–7]. Usually, clinicians consider a combination of pharmacological (like administrating anti-inflammatory drugs, glucosamine, chondroitin sulfate, hyaluronic acid) and non-pharmacological therapies to manage osteoarthritis. If the therapy cannot adequately reduce pain and restore the joint functions, surgical treatments like replacement of damaged joints are called for [5]. As cartilaginous defects are one of the main extrinsic risk factors of osteoarthritis, they must be repaired in the early stage. This can be obtained by regenerative therapies such as allo/autografts, cell-based surgical therapies, and stem-cell stimulation-based methods [5].

Tissue engineering is an important approach in which a biological

* Corresponding author at: Department of Chemical and Biological Engineering, Division of Biomedical Engineering, The Hong Kong University of Science and Technology, Hong Kong, China.
E-mail address: chhkwu@ust.hk (H. Wu).

https://doi.org/10.1016/j.ijbiomac.2022.02.115
Received 1 October 2021; Received in revised form 13 February 2022; Accepted 18 February 2022
Available online 23 February 2022

construct is designed to repair, maintain, or enhance the cartilage function. Despite recent breakthroughs in this field, there remain several challenges like poor integration, phenotypic instability, weak mechanical properties, and inflammation, which must be addressed when transplanting/designing a substitute for cartilage defects [6]. In this work, we address those demands by developing a thermogel based on chitosan, a favorable biomaterial for cartilage repair because its chemical structure is similar to that of cartilage glycosaminoglycans. The good cytocompatibility, low cost, availability, and potential of functionalization by means of hydroxyl and amine groups are other advantages of chitosan. Nonetheless, despite recent progress in chitosan hydrogels for cartilage tissue engineering, there is still the need to improve the physical/mechanical properties and clinical viability [8,9].

Although the mechanical properties of a chitosan hydrogel can be improved by chemical modification using N-(β-maleimidopropyloxy) succinimide ester (BMPS) (Fig. 1a) [10], the shear modulus (76.0 ± 2 kPa) only spans a limited range within the human articular cartilage shear modulus (50–250 kPa). In the current work, we further boost the hydrogel shear properties by using halloysite nanotubes (HNTs) as reinforcements and diclofenac sodium (DS) carriers to suppress inflammation at the damaged site (Fig. 1b). HNTs which are found naturally in nanoscale clay have been utilized in many biomedical and drug delivery applications because of the favorable tubular structure with an inner lumen of ~15 nm and outer diameter of 50–70 nm [11,12]. To address the limited healing capacity of cartilage, kartogenin (KGN), a chondroinductive factor which promotes selective differentiation of mesenchymal stem cells (MSCs) into chondrocytes is introduced. KGN stimulates RUNX1 by releasing the core-binding factor β from filament A, which later forms a complex when binding to this transcription factor in the nucleus. The complex triggers transcription of aggrecan and collagen type II which are important components of the cartilage matrix. Stimulation of RUNX1 in MSCs plays a vital role in their differentiation into chondrocytes and their further proliferation [13,14]. Rapid clearance of KGN from the joint upon administration necessitates to develop a drug delivery system to deliver it gradually. Considering its hydrophobic nature and poor solubility, here starch is used as the drug carrier which has various food and pharmaceutical applications due to its availability, biocompatibility, biodegradability, low cost, processability and possessing hydroxyl groups for functionalization purposes [9,15]. Accordingly, KGN is encapsulated in the hydrophilic monodispersed starch microspheres on a droplet microfluidic chip to improve the therapeutic efficacy (Fig. 1c) and droplet microfluidics provides the mechanism for a uniform drug distribution within the particles, consequently giving rise to more sustained drug delivery and less burst release compared to conventional techniques [16]. To the best of our knowledge, it is the first report on developing KGN-loaded starch microspheres by droplet

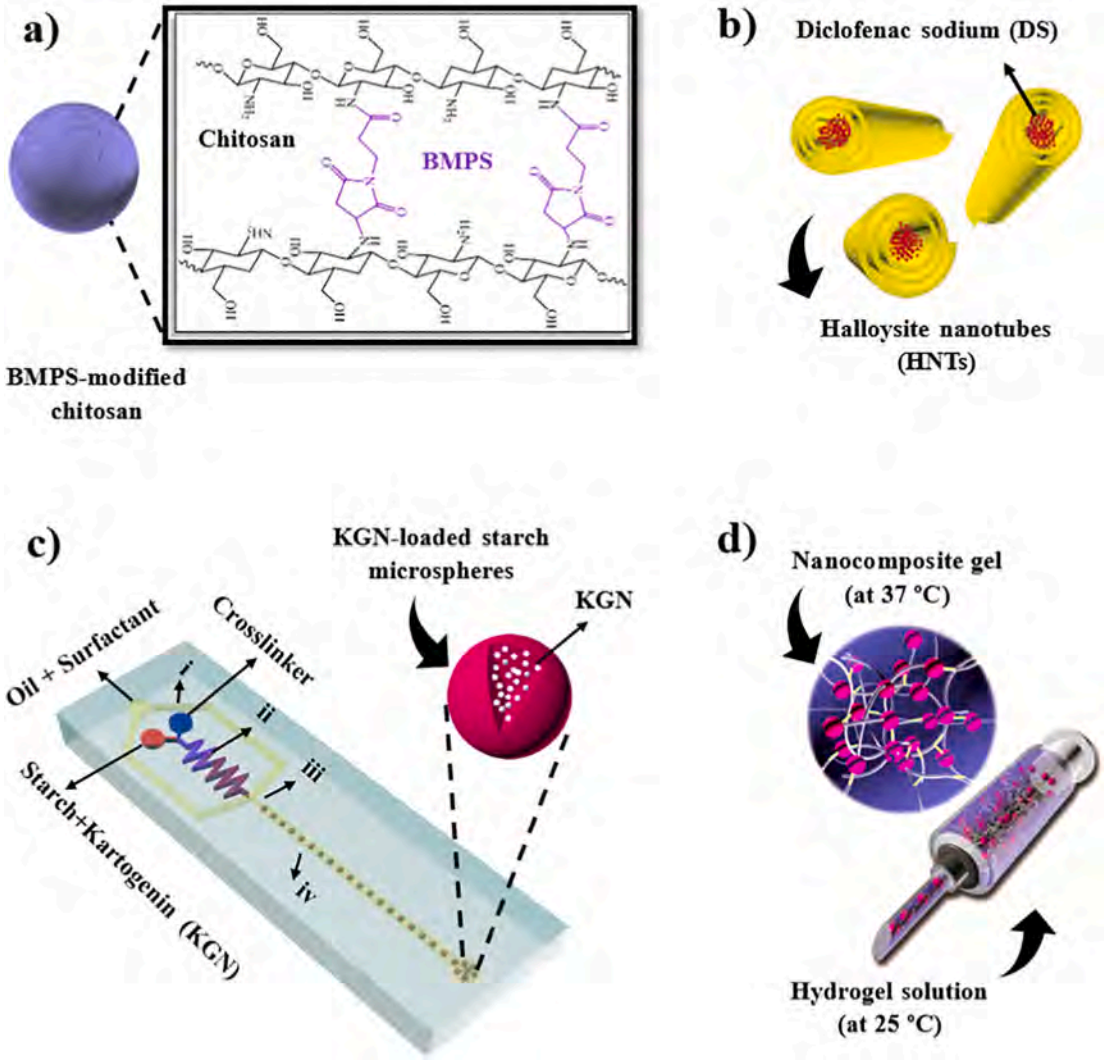

Fig. 1. Schematic illustrations: (a) Modification of chitosan with BMPS, (b) DS-loaded HNTs, (c) Droplet microfluidic chip for preparation of KGN-loaded starch microspheres. The widths of the channels at locations i, ii, iii and iv are 400, 200, 200 and 500 μm, respectively and the height is 300 μm. (d) Current research strategy of cartilage tissue engineering.

microfluidics for cartilage regeneration. These microspheres are combined with the hydrogel to provide a linear KGN release profile to further improve the chondro-inductiveness (Fig. 1d). In this way, a chondro-inductive, anti-inflammatory dual functional nanocomposite hydrogel with a shear modulus (167 ± 5 kPa) comparable to that of native articular cartilage is designed and demonstrated. In addition, this platform is injectable and can be administered to defects with any shape non-invasively. Also, its suitable gelation time (5 ± 0.5 min) at 37 °C improves the clinical viability compared to the previously developed hydrogels which presented gelation times of 10 to over 60 min [10,17–20]. Dual function scaffolds have been developed for simultaneous chondrogenesis using KGN and anti-inflammatory purposes by drugs like DS [21] and curcumin [22]. Despite of their encouraging outcomes in terms of chondrogenesis [21,22], our platform shows less burst release of both drugs with a more linear trend and higher mechanical performance. Based on the superior rheological properties and remarkable capability to continuously deliver biological cues to achieve simultaneous pain relief and chondrogenesis, this smart nanocomposite could be promising for effective management of cartilage defects [10,13,21,23,24].

2. Materials and methods

2.1. Materials

Starch (Cat. No. 03967), HNTs (Cat. No. 685445), trisodium trimeta phosphate (TSTMP, Cat. No. T5508), β-Glycerophosphate disodium salt hydrate (β-GP, Cat. No. G9422), and trichloro(1H,1H,2H,2H-perfluorooctyl)silane (PFOTS, Cat. No. 448931) were purchased from Sigma Aldrich, St. Louis, Missouri, USA. Waitrose brand sunflower oil was obtained from a grocery store. Tween-80 (Cat. No. 8.40123.1000) and Span-80 (Cat. No. 8.22187.0500) were bought from Merck, Kenilworth, N.J., USA. KGN (Cat. No. HY-16268) was purchased from MedChemExpress and DS was obtained from a drug store (manufactured in India by Unique Pharmaceutical Laboratories, A div. of J. B. Chemicals & Pharmaceuticals Ltd). Oligochitosan (MW = 5–10 kDa, Cat. No. P312015) and BMPS (Cat. No. F01022) were provided by Dibo Chemicals Co., Ltd. (Shanghai, China) and Highfine Biotech (Suzhou, China), respectively. The RNA purification kits (PureLink®, Cat. No. 12183018A), one-step quantitative real time polymerase chain reaction (qRT-PCR) kits (SuperScript® III Platinum® SYBR® Green, Cat. No. 11736-051), and PCR primers were obtained from Thermo Fisher Scientific and China Beijing Genomics Institute (Shenzhen, China), respectively.

2.2. Preparation of KGN-loaded starch microspheres

A droplet microfluidic chip (Fig. 1c) was fabricated using a Miicraft 3D printer. The 3D printed structure was heated to 130 °C for 1 day and then coated with PFOTS. The PDMS precursor with a 10:1 weight ratio of prepolymer to curing agent was casted on the mold and incubated at 80 °C for 3 h. Afterwards, the PDMS replica was peeled off from the mold and holes were created at its inlet and outlet using a punch. A thin layer of PDMS (26 μm) was spin-coated at 2000 rpm on a glass plate using the PDMS precursor (10:1) which was then cured at 80 °C for 3 h. The PDMS-coated glass plate and PDMS replica were irreversibly bonded by plasma treatment (PDC-32 G, Harrick Plasma) for 30 s at a power of 18 W. Finally, the assembled chip was heated for 10 min at 80 °C. The widths of the channels shown in Fig. 1c at locations i, ii, iii and iv are 400, 200, 200 and 500 μm, respectively and the height is 300 μm.

Sunflower oil was used as the continuous phase together with 5 wt% surfactants (weight ratio of Span-80: Tween-80–84:16) to stabilize the generated droplets. A 3.5 wt% starch solution was mixed with the proper amount of NaOH (at 40 °C) to increase the solution pH required for crosslinking. A 5 wt% TSTMP solution was prepared as the crosslinker. The water phase, including the starch and crosslinking solutions and oil phase, were injected through the microfluidic inlets at flow rates of 750 and 3000 μL/h, respectively, by means of syringe pumps. The crosslinker and starch solutions were mixed on the chip by a zigzag channel followed by droplet formation with a flow-focusing geometry (Fig. 1c). The starch droplets were crosslinked on the chip and collected from the outlet afterwards to be separated from oil by centrifugation (10,000 rpm, 15 min). After washing several times with ethanol and deionized water, they were freeze-dried for further investigations.

To make the KGN-loaded microspheres, 20 mM KGN (in DMSO) was added to the starch solution (under basic condition) to reach a final concentration of 200 μg/mL and stirred for 3 h before introduction to the chip. After separation of the drug-loaded particles, the supernatant was stored for the encapsulation efficiency (EE) analysis.

2.3. Preparation of DS-loaded HNTs

The HNTs (4 g) were sonicated in 100 mL of Milli-Q water to remove impurities. The particles were collected by centrifugation and ultrasonically dispersed in 100 mL of HCl (1 M) for 30 min. The suspension was magnetically stirred at 50 °C for 2 days and the nanotubes were collected and rinsed with Milli-Q water. The HNTs were then dried in a vacuum oven at 40 °C [12]. For DS encapsulation, 6 mg of DS were dissolved in 25 mL of ethanol and 25 mL of Milli-Q water. 4 g of HNTs were sonicated for 30 min in the drug solution and magnetically stirred for 3 h. DS was then loaded into the nanotubes using three cycles of vacuum pumping (in/out, 30 min) to increase the EE by replacing the air trapped in the lumen of HNTs by the drug molecules [25]. The particles were collected (the supernatant was stored for the EE analysis), washed with Milli-Q water, and dried in a vacuum oven at 35 °C overnight.

2.4. Preparation of thermosensitive chitosan-based hydrogels

Oligochitosan was chemically modified with BMPS as described previously [10,26]. Briefly, chitosan was dissolved in hot PBS (~70 °C) by agitation (4 w/v%). After removing the impurities by centrifugation, the solution pH was adjusted to 7.0 with 1 M NaOH. It was blended with BMPS (1.3 g) and agitated at 25 °C for 6 h to produce 20% BMPS-modified chitosan [10,26]. Dialysis against ultrapure water was conducted in the solution for 3 days using a dialysis bag (Spectra/Por® 3, MWCO: 3.5 kDa, Spectrum Laboratories Inc.) and the chitosan concentration was adjusted to 5 w/v% by concentrating the solution using centrifugal filters (Ultracel®, Cat. No. 4302, 3 kDa NMWL, Millipore). After filtering the solution with 0.22-μm filters, it was frozen instantly in liquid nitrogen and kept at −80 °C for further experiments. The chitosan concentration was calculated by measuring the weight of solid chitosan in the 1 mL solution after lyophilization.

To produce the thermogels, β-GP (in Milli-Q water) was blended with BMPS-chitosan as a physical crosslinker to reach a concentration of 14.2 wt% and incubation at 37 °C causes hydrogel gelation. To enhance the mechanical properties of the gel, HNTs (2, 4, 6 and 8 w/v%) were mixed with the hydrogel solution before incubating at 37 °C. To prepare the dual functional nanocomposite thermogel, DS-loaded HNTs (6 w/v%) and KGN-loaded starch particles (1.4 w/v%) were combined with the hydrogel solution and incubated at 37 °C.

2.5. Scanning electron microscopy

Field-emission scanning electron microscopy (FE-SEM, JEOL-6700F) was performed to examine the hydrogel morphology and the particle shape and size.

2.6. Determination of starch particle size

The dynamic light scattering (DLS) technique (Malvern Instruments, Malvern, UK) was utilized to measure the starch particle size and polydispersity indexes.

2.7. Dynamic mechanical analysis

To investigate the mechanical behavior of the hydrogels, an 8 mm parallel plate fixture was mounted on a rheometer (ARES, TA Instruments, New Castle, USA), where the hydrogel disks were placed and examined in the frequency sweep mode (1 to 100 rad/s frequency at 1% strain) and strain sweep mode (1% to 100% strain at 1 rad/s frequency). The experiments were conducted at 37 °C and the storage shear modulus at 1 rad/s shear frequency and 1% strain was considered in the data analysis. Oscillatory measurements were carried out to determine the hydrogel gelation time and temperature. Aliquots of the hydrogel precursor solutions were introduced between the concentric cylinders of the rheometer and to avoid sample evaporation, the system was shielded with mineral oil. To determine the gelation time, the evaluation was conducted at 1 Hz frequency and 37 °C. To measure the gelation temperature, the frequency was adjusted to 1 Hz while the temperature was altered from 20 up to 60 °C with a rate of 1 °C/min. The time/temperature where G' and G'' followed a power law ($G' \propto \omega^n$ and $G'' \propto \omega^n$) with the same n exponent were chosen as the gelation time/temperature [7,10].

2.8. Encapsulation efficiency and in vitro release tests

To measure the %EEs of the drug-loaded particles, the absorbance of DS and KGN in the supernatants collected from the samples were determined at 275 and 278.4 nm, respectively, on the Varikosan™ LUX multimode microplate reader. The %EE was measured according to Eq. (1) [7,21]:

$$EE(\%) = \frac{Drug_{total} - Drug_{Unloaded}}{Drug_{total}} \times 100 \quad (1)$$

The drug release kinetics was determined by recording the absorbance of KGN and DS at 278.4 and 275 nm, respectively. 8 mg of the KGN-loaded starch microspheres and 33.6 mg of the DS-loaded HNTs were immersed in 2 mL of PBS (pH = 7.4) by transwell inserts. The nanocomposite thermogel (containing 8 mg of KGN-loaded starch microspheres and 33.6 mg of DS-loaded HNTs) was immersed in 2 mL of PBS. At certain time intervals, the released medium (at 37 °C) was tested and fresh PBS was added to each well until the final measurement. The standard absorbance calibration curves of KGN and DS were established to calculate the drug release percentage using Eq. (2) in which M_t is the quantity of the released drug at time t and M_i is the quantity of the initial drug in the sample [7,15].

$$Drug\ release\ (\%) = \frac{M_t}{M_i} \times 100 \quad (2)$$

Thermogel-KGN (non-reinforced hydrogel mixed with the same amount of KGN in the KGN-loaded starch particles) and thermogel-DS (non-reinforced hydrogel mixed with the same quantity of DS in the DS-loaded HNTs) were prepared and drug release was determined for comparison.

2.9. Biological studies

2.9.1. Cell culture

Human adipose MSCs (hAMSCs, Cat. No. PCS-00-011, ATCC) were used in the biological studies. A basal growth medium (Cat. No. PCS-500-030, ATCC) supplemented with a growth kit (Cat. No. PCS-500-040, ATCC) was employed to culture the cells. The complete medium contained 2% FBS, 5 ng/mL rh FGF basic, 5 ng/mL rh FGF acidic, 5 ng/mL rh EGF and 2.4 mM L-Alanyl-LGlutamine. The cells were incubated at 37 °C with 5% CO_2 and the culture medium was changed every 2 days. After the cells reached 80% confluence, they were detached by trypsin (0.05 w/v%)/EDTA (0.53 μM) and sub-cultured until passage 8. The cells were seeded onto 24-well plates with the seeding density of 10^4 cells per well and cultured for the *in vitro* cytocompatibility investigation.

2.9.2. Cytocompatibility assays

To evaluate the particles cytocompatibility, the DS-loaded HNTs (8.4 mg) or KGN-loaded starch microspheres (2 mg) were immersed in 2 mL of the cell culture medium and incubated with hAMSCs using transwell inserts (Millicell Hanging Cell Culture Insert, Cat. No. MCHT24H48, Merck) (Fig. S1). After 48 h, live/dead staining was performed by adding propidium iodide and fluorescein diacetate (10 μg/mL) to the culture medium. After incubation for 30 min, the medium was removed and the cells were washed with the culture medium. Afterwards, fluorescence images were taken and the cell viability was determined as the percentage of live cells using ImageJ. To study the cytocompatibility, the cells were exposed to the hydrogel solution (concentration of precursor solution in culture media: 10 mg/mL) and/or extract of ~150 μL hydrogel in 2 mL of the cell culture medium for 48 h before conducting live/dead staining.

2.9.3. In vitro chondrogenic differentiation

In vitro chondrogenic differentiation was performed by micromass culturing of hAMSCs. The cells were expanded up to 5×10^6 cells per seeding and detached by trypsinization and centrifugation (5 min at 600 rpm) was conducted on the cell suspension to produce a cell pellet. The pellet was resuspended in 500 μL of the chondro-inductive medium (Cat. No. PCS-500-051, ATCC) and 20 μL of the cell suspension (containing 0.2×10^6 cells) were introduced to the middle of each well on a 24 well-plate, followed by incubation for 3 h at 37 °C (5% CO_2). The chondrogenic medium (2 mL) was supplemented to each well and refreshed every other day. To examine the effects of the microspheres on chondrodifferentiation of hAMSCs, KGN-loaded particles (2 mg) were incubated with the cell pellets using transwell inserts. The particles were placed on the upper part of the insert and dispersed in 2 mL of the chondrogenic medium, while the medium in the lower part was changed every other day. 150 μL of the nanocomposite thermogel were submerged in 2 mL of the chondrogenic medium to prepare the nanocomposite extract. At certain time points, the medium containing the extract was collected to treat the cells and the nanocomposite was immersed in the fresh medium until the last time point. The cell pellets were cultured for 21 and 14 days to conduct PCR analysis and immunofluorescence staining (Supporting information, SI), respectively. The cell pellets were also exposed to pure KGN to compare with the gene expression results of the KGN-loaded starch particles. The KGN concentration in the cell culture medium was adjusted according to the drug release curve from the microspheres. The cells with no treatment served as the control. The GAG/DNA contents in the cells were examined after treatment for 21 days. After digestion of the cell pellets with a papain solution, the DNA content and sulfated glycosaminoglycan (s-GAG) were quantified using a Picogreen assay (Cat. No. P11496, Thermo Fisher) and Blyscan kit (Biocolor, Carrickfergus), respectively (SI). Cell proliferation was examined after treatment for 1, 3, 5, and 7 days by the WST-1 cell proliferation assay kit (Cat. No. ab65473, Abcam) according to the manufacturer's protocol [7,10].

2.9.3.1. qRT-PCR analysis. RNA extraction was conducted on the hAMSC pellets treated with different samples by an RNA purification kit and a NanoVue Plus spectrophotometer (Bichrom) was employed to quantify the RNA concentrations. The gene expression levels were measured with a one-step qRT-PCR kit (SI) and PCR machine (LightCycler® 480 Instrument II, Roche, Basel, Switzerland). The expressions of collagen type I (COL1A1), collagen type II (COL2A1), collagen type X (COL10A1), SOX9, and aggrecan genes were analyzed. Glyceraldehyde-3-phosphate dehydrogenase (GAPDH) was employed as an internal control. The delta-delta C_t method was adopted to estimate the relative normalization ratio of the PCR products resulting from each target gene and the values were normalized *versus* the non-treated sample (as

control) and shown as fold changes. The primer sequences are presented in Table S1.

2.10. Statistical analysis

All the experiments were conducted in triplicate and the results were presented as mean ± standard deviation. The results statistical significance was determined by analysis of variance (ANOVA single factor) which was set at $P < 0.05$ (*).

3. Results and discussion

3.1. Starch microspheres

A zigzag channel is employed as a micro-mixer in the microfluidic device which is able to generate chaotic advection by recirculation around turns to produce efficient mixing of the reagents. Formation of uniform starch particles can be explained by the following mechanisms. A concentration gradient occurs at the interface of the TSTMP and starch solutions when they collide at high rates, leading to nucleation as a

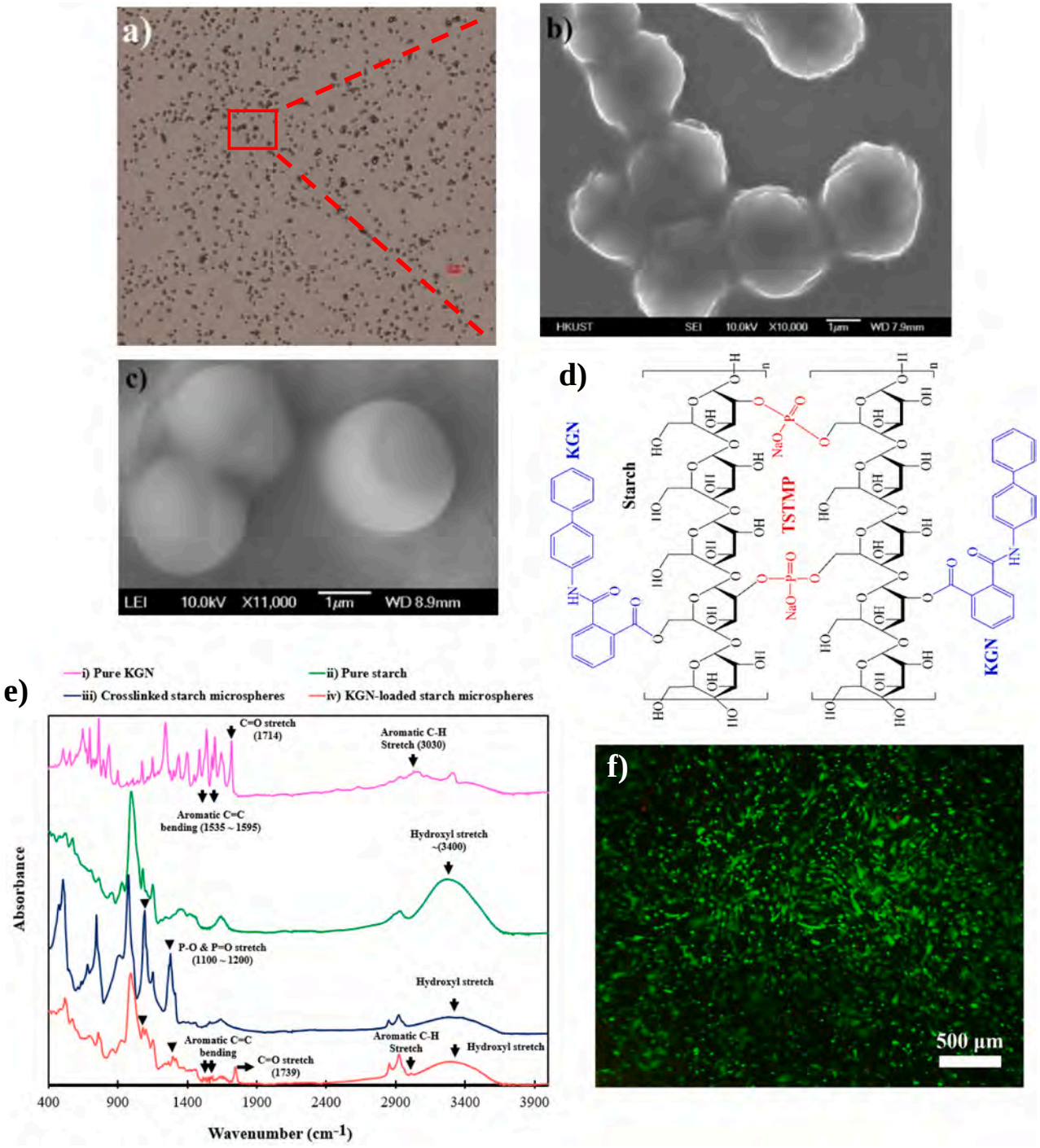

Fig. 2. (a) Optical microscopy (scale bar: 20 μm) and (b) FE-SEM images of the bare starch microspheres. (c) FE-SEM and (d) Chemical structure of KGN-loaded starch microspheres. (e) ATR-FTIR spectra of i-pure KGN, ii-pure starch, iii-crosslinked starch microspheres and iv-KGN-loaded starch microspheres. (f) Live/dead staining of hAMSCs treated with KGN-loaded particles for 48 h (scale bar: 500 μm).

result of the crosslinking reaction in a short time. The reaction time for seed formation is smaller than the growth time to develop larger particles. Thus, a stream carrying lots of seeds is formed and enters the oil phase through the orifice. High flow rates create a narrow jet regime in which a continuous thread of the water phase extends into the outlet channel and breaks downstream of the orifice. This narrow jet is unstable due to Rayleigh-Plateau instability and will further turn into droplets with dimensions significantly smaller than the orifice width. Each droplet is stabilized by the oil phase containing surfactants in the surrounding, which provides a uniform environment for the seeds to grow at similar rates leading to highly monodisperse particles [27–29].

The size of the bare particles is 2.8 ± 0.7 μm with a polydispersity index of 0.2 (Fig. 2a & b), which becomes 2.2 ± 0.4 μm (polydispersity index: 0.1) after KGN encapsulation (Fig. 2c) with EE of 80.49 ± 3%. The particles have a smooth surface and uniform spherical shape without pores. The compact surface morphology and x-ray diffraction (XRD) (SI, Fig. S2) confirm efficient crosslinking [9,15]. Fig. 2d illustrates the chemical structure of crosslinked starch microspheres loaded with KGN. Besides the physical entrapment of KGN molecules within the microspheres upon rapid crosslinking reaction on the chip, the carboxyl groups in KGN react with hydroxyl groups of the starch chains under the basic condition [30,31] and by further mixing this solution with TSTMP, phosphate groups react with free starch hydroxyl groups to produce crosslinked drug-loaded particles (Fig. 2e). The absorption peaks at 3030 and 1714 cm^{-1} of pure KGN are related to aromatic C—H and C═O stretching, respectively, which shift to 3018 and 1739 cm^{-1} in the FTIR pattern of the KGN-loaded starch particles [21]. The peaks at 1535–1595 cm^{-1} are assigned to KGN aromatic C═C bending as shown in the FTIR spectra of the KGN-loaded particles. Typical stretching of P═O and P—O are seen from both the bare and KGN-loaded particles at 1100–1200 cm^{-1}. However, the intensity is reduced in the KGN-loaded particles compared to the bare ones, indicating a smaller crosslinking density due to the reduction of free hydroxyl groups in starch (because of interaction with KGN). The intensity of the peak related to starch hydroxyl stretching vibration at 3400 cm^{-1} is reduced in both bare and drug-loaded particles compared to pure starch on account of crosslinking *via* hydroxyl groups [32]. The swelling percentage of the microspheres (Fig. S3) increases after drug loading probably due to the lower crosslinking densities of drug-loaded particles. Upon immersing the drug-loaded starch particles in PBS, they absorbed the liquid immediately and the rate of water uptake was high in the first 8 days. Following that, the swelling percentage did not change significantly in the next days, and the microspheres reached their swelling equilibrium (swelling percentage: ~450%) and finally a slight reduction in water uptake was seen after 13 days (Fig. S3). Live/dead staining of the hAMSCs treated with KGN-loaded starch microspheres for 48 h (Fig. 2f) indicates suitable biocompatibility of the particles with hAMSCs, confirming that the KGN release level (~470 nM) from the microspheres is safe for the cells [10,14].

3.2. DS-loaded HNTs

The FTIR spectra of the pure HNTs, pure DS and DS-loaded HNTs are exhibited in Fig. 3a which reveals characteristic peaks of DS and HNTs (explained in SI) without significant shifting suggesting that there is no chemical interaction between DS and HNTs. Therefore, the DS molecules

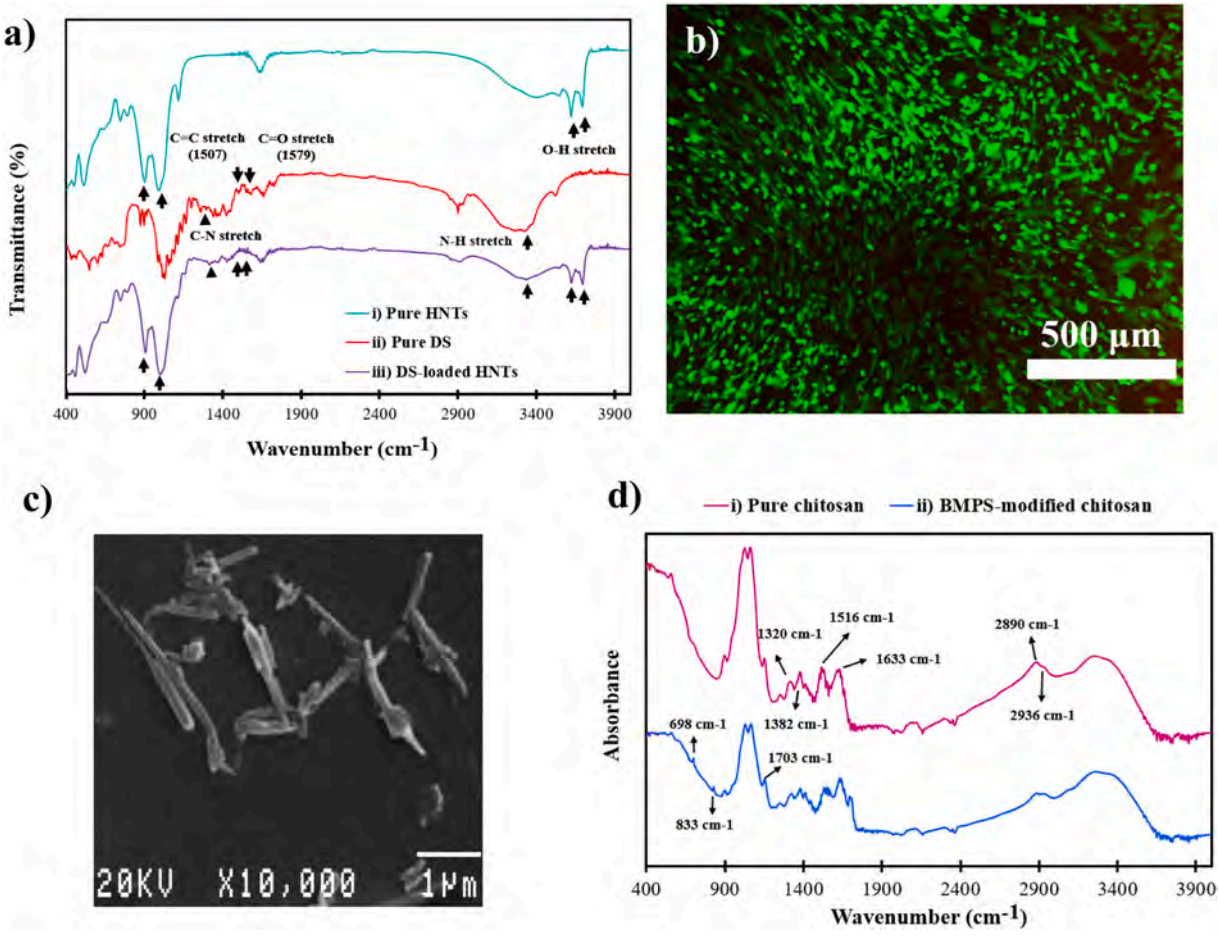

Fig. 3. (a) ATR-FTIR spectra of i-pure HNTs, ii-pure DS, and iii-DS-loaded HNTs. (b) Live/dead staining of hAMSCs treated with DS-loaded HNTs for 48 h (scale bar: 500 μm). (c) FE-SEM image of DS-loaded HNTs. (d) ATR-FTIR results of i-pure and ii-BMPS-modified chitosan.

are mechanically entrapped within the hollow nanotubes by vacuum pumping [33]. The *in vitro* cytocompatibility tests (Fig. S4 & Fig. 3b) indicate that while HNTs are cytocompatible with hAMSCs, the DS release level (2.6 μM within 48 h) does not produce any cytotoxic effects [34]. The cells can internalize HNTs *via* clathrin and caveolae-dependent endocytosis. After HNTs enter the cells, they form aggregates in the perinuclear cell region without any adverse effects on proliferation. While HNTs can be transported by both Golgi apparatus and lysosomes, actin filaments and microtubules are also involved in the transport pathway [35–37]. Naumenko et al. [35] shave shown that not only the HNT-doped hydrogels have the suitable biocompatibility and biodegradability (excellent resorption within 6 weeks) *in vivo*, but also implantation in rats forms new blood vessels around the injury sites. Hence, HNTs are promising candidates for drug delivery and Fig. 3c indicates the morphology of the DS-loaded HNTs.

3.3. Thermosensitive chitosan-based hydrogels

Chitosan is chemically modified with BMPS and the hydrogel mechanical properties are improved significantly as verified by our previous experiments [10]. The successful reaction between the chitosan amino groups with BMPS maleimidyl groups through Michael-type addition is confirmed by FTIR (Fig. 3d). The absorption bands at 1320, 1382, 1516, and 1633 cm^{-1} from chitosan are related to amide III band, -CH_2 bending, amide II and amide I bands, respectively. The -CH_2 and -CH_3 aliphatic groups shows peaks at 2936 and 2890 cm^{-1}, respectively. The maleimide related absorption bands in BMPS-chitosan including alkenyl C—H out of plane bending, ring deformation, and imide I band at 833, 698, and 1703 cm^{-1}, respectively, indicate effective maleimide conjugation with the chitosan backbone [10,26].

To prepare the thermoresponsive hydrogel, we take advantage of the low critical solution temperature (LCST) when chitosan is combined with β-GP (a weak organic base). While the mixture is soluble at T < LCST (which can be tuned near to 37 °C), it gelatinizes when heated due to development of physical junction moieties in the chitosan chains in the chitosan-chitosan hydrophobic interactions [9,10,38]. Although it has been shown [10] that the shear modulus of chitosan hydrogel can be improved to 76 ± 2 kPa by BMPS functionalization, it is not sufficient for defects in the deeper parts of the cartilage, considering the depth-dependence of articular cartilage mechanical properties [39]. Furthermore, this sample has a gelation time of 10 ± 0.6 min at 37 °C [10] which should be reduced to avoid unwanted leakage of the hydrogel solution outside the defect before gelation occurs [9]. Therefore, this formulation serves as the control (Table 1, sample No. 1) and is further reinforced by HNTs to produce better hydrogel rheological properties.

Table 1 shows that the shear modulus of the chitosan hydrogel (sample No. 1) is enhanced significantly with HNTs as reinforcements. There are also reduction effects on the hydrogel gelation time and temperature. HNTs have proper compatibility with chitosan hydrogels because of the negatively charged silicate outer surface which can interact with positively charged chitosan amino groups. Consequently, HNTs and chitosan can form complexes by electrostatic attraction and HNTs produce physical crosslinking effects for the hydrogel acting as crosslinking nodes in the gel network [40,41]. Therefore, hydrogels with a higher HNT content gelatinize faster and exhibit a lower gelation temperature [42]. However, the drop in the shear modulus at the highest filler concentration may stem from the nanotube agglomeration in the hydrogel acting as stress concentration points [9,43,44]. As 6 w/v% HNTs results in the highest shear modulus, this filler content is considered in subsequent DS-loading to be combined with the hydrogel for dual drug delivery purposes.

Table 1
Rheological properties of hydrogels with different filler contents.

Sample no.	HNTs (w/v %)	Starch microspheres (w/v%)	Gelation time (min)	Gelation temperature (°C)	Storage shear modulus (kPa)
1	0	0	10 ± 0.6	37.9 ± 0.7	76.0 ± 2
2	2	0	8 ± 0.5	36.8 ± 0.3	103 ± 7
3	4	0	7.3 ± 0.6	36.5 ± 0.5	128 ± 6
4	6	0	5.7 ± 0.3	36 ± 0.3	160 ± 8
5	8	0	5 ± 0.5	35.8 ± 0.6	110 ± 12
6	6	1.4	5 ± 0.5	36 ± 0.7	167 ± 5

3.3.1. In vitro drug release

Rapid clearance of KGN from the synovial cavity limits the therapeutic effectiveness after direct injection into the joint at a high dosage. Therefore, a drug delivery system with controlled and prolonged KGN release is desired [7]. It is also preferable to modulate inflammation in a destructive joint with fewer injections of anti-inflammatory drugs. Herein, a chondro-inductive, anti-inflammatory dual functional nanocomposite thermogel (sample No. 6) is prepared by incorporating KGN-loaded starch particles (1.4 w/v%) and DS-loaded HNTs (6 w/v%) in the hydrogel. The KGN release profile from (i) Thermogel-KGN (non-reinforced gel mixed with the same amount of KGN in the microspheres for comparison) [10], (ii) KGN-loaded starch microspheres, and (iii) nanocomposite thermogel, are illustrated in Fig. 4a. Not only does KGN encapsulation in the starch microspheres hinder burst release significantly, but also it provides much slower drug release kinetics over a month compared to Thermogel-KGN [10]. Swelling behavior of the drug-loaded microspheres which is mediated by their crosslinking density, significantly affects the ester bonds hydrolysis responsible for KGN release. Immersion of the particles in PBS and the subsequent fast water penetration into them within the first days helps the polymeric chains to loosen up which facilitates the KGN diffusion through the starch chains. Thus, the drug release is controlled by swelling in this stage. Once the particles' swelling reaches the equilibrium state, the KGN diffusion will be more steady and slower. Therefore, swelling and hydrolysis of the ester bonds responsible for KGN conjugation to the starch chains occurred at a slower rate (at neutral pH) in the following days. This could extend the KGN bioavailability and chondrogenic efficiency as it can be uptaken by the cells more gradually to regenerate cartilage. In this case, the hydrolysis, degradation and erosion of the particles from surface or a complex mechanism involving swelling and degradation govern the KGN diffusion and release [45]. Not only the particles' swelling ability regulates their chondro-inductiveness, but also, it can accelerate the tissue healing rate by providing a moist environment in the cartilage lesion similar to native tissue with efficient nutrition transfer for the host cells to attach and grow [45,46]. More importantly, the monodispersity of the particles with homogenous drug distribution within the network achieved by the droplet microfluidic approach causes more regulated KGN release than Thermogel-KGN. To the best of our knowledge, it is the first report on producing KGN-loaded starch microspheres by droplet microfluidics for cartilage repair. Considering the prolonged KGN release profile without significant burst release together with the small size, they have large potential for injection into defects [16]. Further incorporation of the same quantity of KGN-loaded particles in the gel reduces burst release and the cumulative release profile is almost linear in this case (sample No. 6). This can be explained by that the hydrophobic KGN molecules should penetrate through the hydrophilic thermogel network when released from the incorporated starch particles giving rise to a longer transport time. As a result, KGN is released continuously in a more regulated manner from the nanocomposite gel for over a month to boost its therapeutic efficacy. Compared to reported KGN-loaded chitosan-based particles [13], scaffolds [47,48] or hydrogels [23,49], our nanocomposite thermogel delivers KGN in a more prolonged and controlled way with less burst release.

Similarly, DS encapsulation in HNTs decreases burst release and retards dissolution compared to Thermogel-DS (non-reinforced gel mixed with the same content of DS in HNTs) (Fig. 4b). Incorporation of

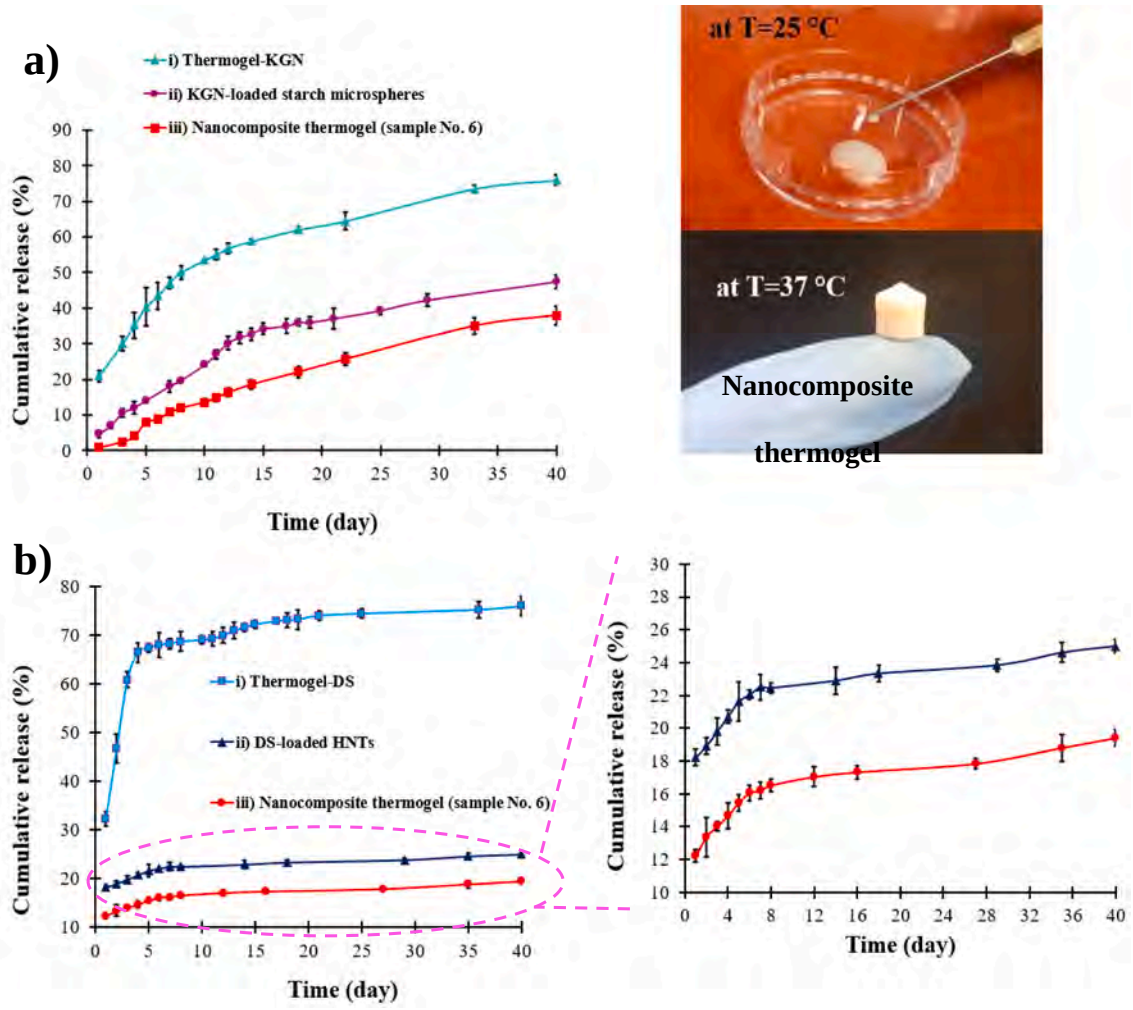

Fig. 4. (a) KGN release profile from i-Thermogel-KGN (non-reinforced gel mixed with the same KGN amount in particles) [10], ii-KGN-loaded starch microspheres, and iii-nanocomposite thermogel. (b) DS release profile from i-Thermogel-DS (non-reinforced gel mixed with the same quantity of DS in HNTs), ii-DS-loaded HNTs, and iii-nanocomposite thermogel.

the same quantity of DS-loaded HNTs in the hydrogel (sample No. 6) further reduces burst release and the release rate for over 40 days. This is because after DS molecules have migrated from the nanotube inner lumen, they penetrate the hydrogel network and are released to the medium. As this platform releases DS in a more gradual and extended fashion than previously developed DS delivery systems [50,51], it may overcome the limitation of DS rapid systemic clearance which usually necessitates several administrations per day for chronic inflammation [33]. However, further investigations are needed to verify its anti-inflammatory action. All in all, the nanocomposite gel co-delivers KGN and DS sustainably for more than 40 days thus eliminating the need for repetitive injections.

3.3.2. *Morphology, cytocompatibility, rheology, swelling and degradation evaluations*

The FE-SEM images (Fig. 5a–c) of the freeze-dried hydrogels indicate that the nanocomposite has smaller pores than the non-reinforced hydrogel due to the presence of the particles in the network acting as crosslinking nodes. The porous structure with interconnected porosities seems to be appropriate for nutrient transport. Suitable dispersion of both drug carriers in the nanocomposite is evident as shown in Fig. 5b & c suggesting homogenous drug release and mechanical properties. The *in vitro* results indicate that the nanocomposite thermogel is cytocompatible and has no adverse effect on hAMSCs (Fig. 5d). The release levels of KGN and DS from this platform are 100 nM and 1.8 μM, respectively.

The nanocomposite shear modulus of 167 ± 5 kPa (Fig. 6a–b) spans a broader range of equilibrium cartilage shear modulus (50–250 kPa) compared to the chitosan-based gels developed previously [8,10,49]. Considering the spatial variations in cartilage shear properties [39], this hydrogel is beneficial to functional engineering of cartilages with defects in deeper parts, probably down to the middle zone to support loading after injection. The cartilage middle zones have complex composition and collagen fibril alignments rendering unique shear-resistant properties. The shear stress response from the cartilage stems from stretching of collagen fibrils with a random distribution [39,52].

The gelation time and temperature (Fig. 6c–d) are 5 ± 0.5 min and 36 ± 0.7 °C, respectively, thereby offering a more manageable system for clinical practice compared to other hydrogels [10,19,20,49]. It also provides sufficient time for operation while obviating the need to keep tissues immobilized for a long time after injection. The swelling coefficient of the nanocomposite increased considerably (~12% after 7 days) compared to the non-reinforced hydrogel due to the high swelling ability of the embedded starch microspheres. Thus, we should consider the particles' swelling percentage and its impact on the overall nanocomposite swelling to roughly estimate the initial volume of the needed hydrogel depending on the lesion size to avoid any probable inflammation [45,46].

Adjusting the scaffolds degradation rate to the healing rate of the target tissues is of a great importance to design scaffolds with better *in vivo* stabilities and avoid their catastrophic and immediate failure upon

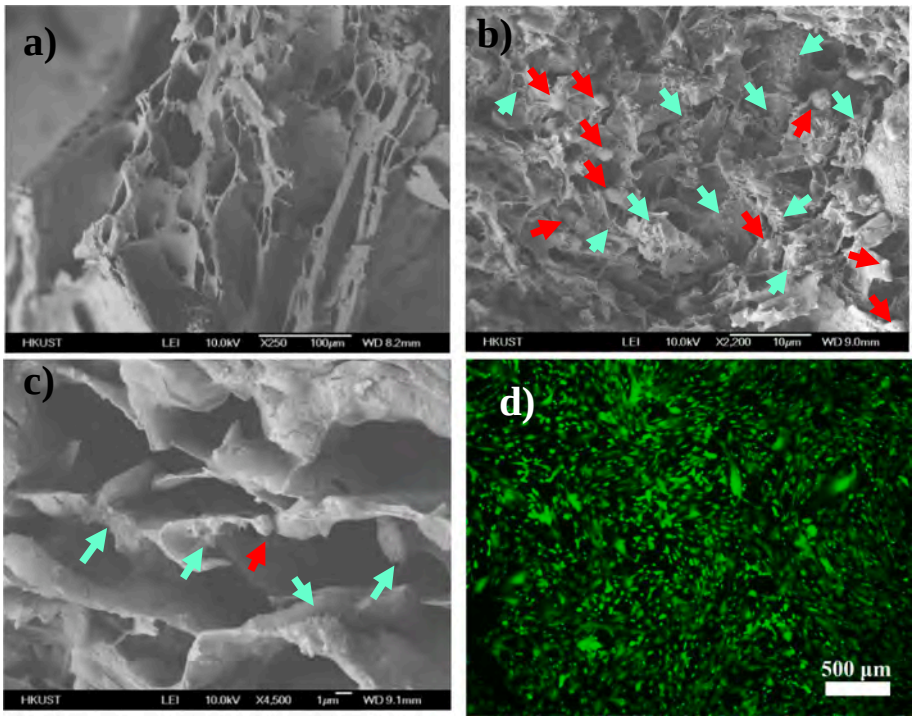

Fig. 5. FE-SEM images of (a) Non-reinforced hydrogel and (b) & (c) Nanocomposite thermogel. The green and red arrows display dispersion of DS-loaded HNTs and KGN-loaded starch particles in the nanocomposite, respectively. As shown in (c), both particles act as crosslinking nodes in the thermogel. (d) Live/dead staining of hAMSCs treated with the nanocomposite thermogel for 48 h.

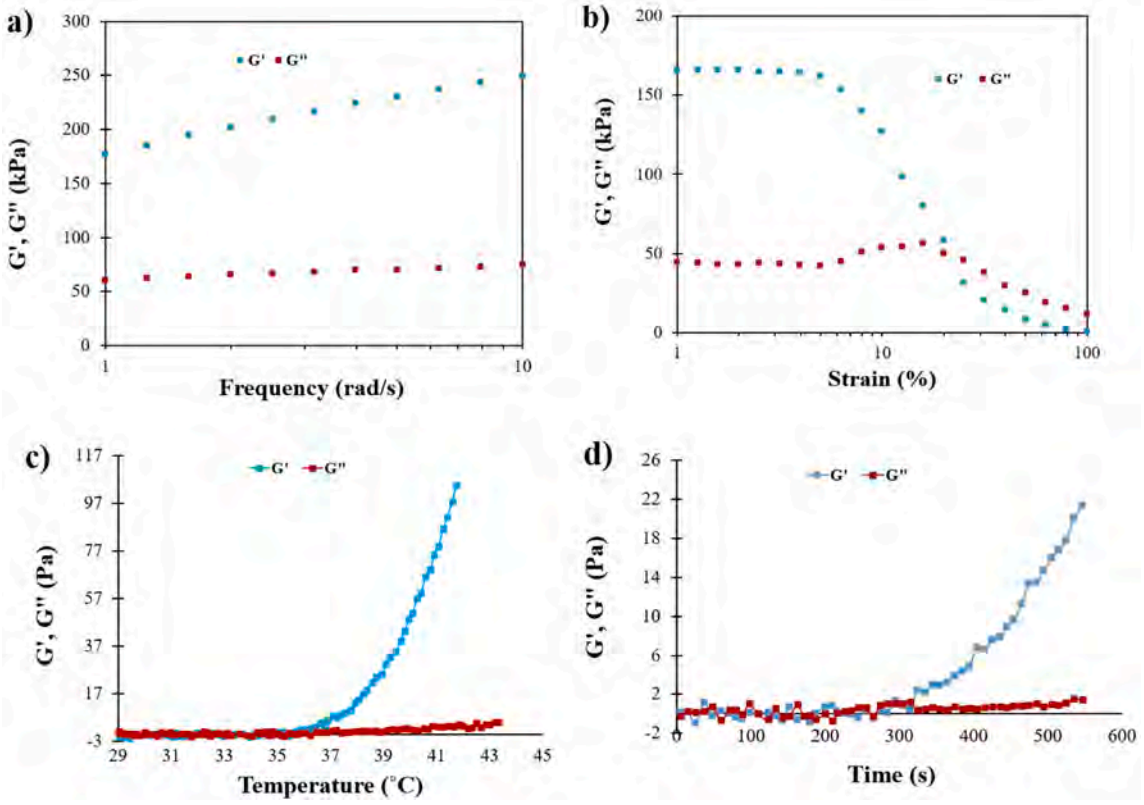

Fig. 6. Dynamic mechanical properties of the nanocomposite thermogel: (a) Frequency sweep mode (at 1% strain) and (b) Strain sweep mode (at 1 rad/s frequency). Determination of gelation: (c) Temperature and (d) Time (at 37 °C).

implantation. Limited degradability of HNTs makes them attractive to be used as nanofillers in polymeric scaffolds with the aim of slowing down their enzymatic degradation rate. Other than limited degradability of HNTs, they act as physical crosslinkers in hydrogels and decrease their water uptake which causes less exposure of the polymeric chains to the degradation medium. Consequently, less hydrolysis and degradation of the hydrogels will occur [53,54]. Therefore, although HNTs are non-degradable at a neutral pH and 37 °C, their combination with chitosan and starch which degrade enzymatically when exposed to lysozyme (available in human cartilage ECM) and α-amylase (existing in human fluids), respectively provide us a suitable biodegradable platform [10,35,36,55,56]. The *in vitro* degradation trend of the nanocomposite thermogel (SI, Fig. S5) implies that it is not likely to degrade entirely in one month and degradation arises mainly through the surface [10]. It should be noted that, the rates of the nanocomposite swelling and enzymatic degradation also influence the KGN release profile and bioefficacy which directly regulates cartilage regeneration rate besides governing the hydrogel volume change over time. All in all, the rate of nanocomposite enzymatic degradation should match the rate of tissue regeneration *in vivo* to achieve optimal cartilage healing and eliminate the risk of further inflammation in the cartilage lesion in long periods [46].

3.3.3. *In vitro chondrogenic differentiation*

Fig. 7a presents the qRT-PCR results related to mRNA of hAMSCs exposed to pure KGN, KGN-loaded starch microspheres and nanocomposite thermogel for 21 days. All the samples upregulate the expressions of the chondrogenic marker genes including COL2A1 (primary ECM element in articular cartilage), SOX9 (an essential factor of chondrogenesis which directly transactivates COL2A1), and aggrecan (the main articular cartilage proteoglycan provides load-bearing properties due to the highly hydrated structure) [14,23,57]. KGN encapsulation in the starch microspheres enhances the expression levels of COL2A1, SOX9 and aggrecan in hAMSCs significantly compared to the pure KGN sample in which the cells are treated with a similar KGN concentration released from the microspheres. Since KGN is a hydrophobic small molecule with weak bioavailability, the therapeutic efficiency is governed by the release profile. Accordingly, KGN produces superior chondrogenic effects on hAMSCs after conjugation with the starch microspheres. The water solubility and permeability are elevated and delivery is gradual. Further incorporation with a similar quantity of KGN-loaded particles in the hydrogel enhances the gene expression levels of COL2A1, SOX9, and aggrecan considerably, because the more controlled/linear release profile of KGN from the nanocomposite boosts the KGN bioavailability and therapeutic efficacy more than the starch microspheres. As a result, the KGN regenerative effectiveness improves substantially when delivered linearly in a continuous manner [13]. Moreover, the relative expressions of COL1A1 and COL10A1 (biomarker of hypertrophic chondrocytes) remain unchanged under all conditions. Therefore, although the cells treated with each KGN containing samples display better chondrogenic differentiation than the control, the nanocomposite thermogel is the most powerful in promoting chondrogenesis in hAMSCs. Besides the upsurge in expression of chondrocyte markers, the GAG/DNA content increases up to 2 times when the cell pellets are

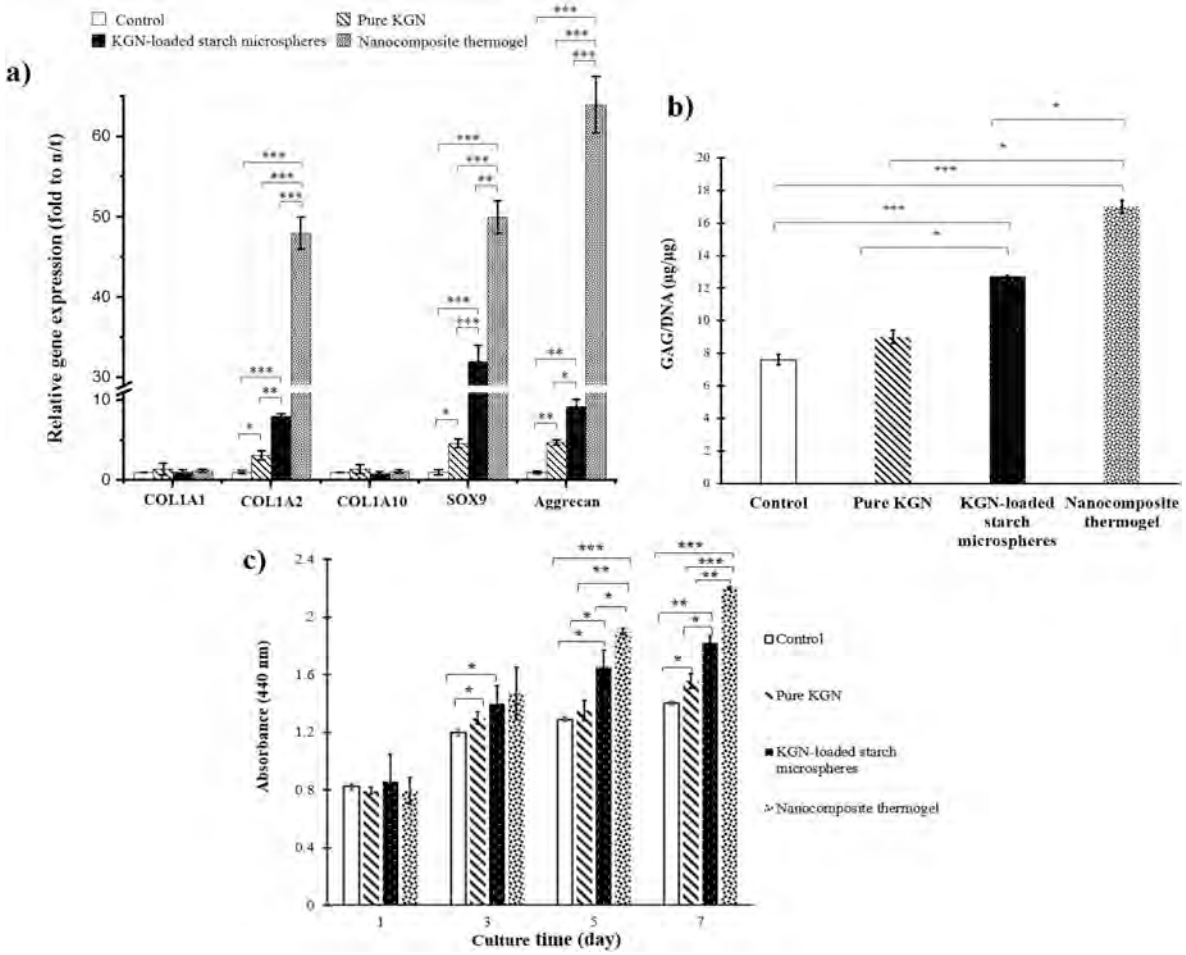

Fig. 7. (a) qRT-PCR results of COL1A1, COL2A1, COL10A1, SOX9 and aggrecan (results displayed in fold-change relative to control) and (b) GAG per DNA content after cell culturing for 21 days. (c) Cell proliferation after 1, 3, 5 and 7 days for hAMSCs untreated (control) or treated with pure KGN (with similar drug concentration released from starch particles), KGN-loaded microspheres, and nanocomposite thermogel (*$p < 0.05$, **$p < 0.001$, ***$p < 0.0001$).

exposed to the nanocomposite compared to the pure KGN or control (Fig. 7b). Although GAG deposition in the cells cultured with KGN-loaded microspheres is lower than that treated with the nanocomposite, it was still noticeably higher than that cultured with pure KGN. Fig. 7c shows the positive impact of KGN on cell proliferation up to 7 days. KGN encapsulation in the microspheres enhances cell proliferation and integration with the hydrogel produces the best results. Enhancement effect of KGN on cell proliferation has been seen on different cell types including MSCs and chondrocytes previously [7,10,58,59]. Liu et al. [58] revealed that, exposure of cartilage stem/progenitor cells (CSPCs) to KGN elevates the cell growth and reduces the apoptosis percentage. To investigate the underlying mechanism, they performed comprehensive transcriptomics investigations on KGN-treated CSPCs. It was indicated that, KGN enhances the secretion of IL-6 by which the phosphorylation of Stat3 is activated. Other than IL-6/Stat3 signaling pathway, activation of TGFβ pathway by KGN during chondrogenic induction of MSCs mediates cell proliferation and cartilage regeneration. Decker et al. [59] demonstrated that, upregulation of genes encoding TGFβ and hedgehog by KGN plays vital role in development of cartilage nodules. Both hedgehog and TGFβ boost the chondrocytes proliferation through crosstalk with PTHrP during mouse limb development [58,59]. Our results indicate that once KGN is delivered more gradually by being encapsulated in the particles or nanocomposite hydrogel, a significant higher proliferation rate can be achieved than supplementing the cell culture media with similar KGN contents immediately. This suggests that, the hydrophobic nature of KGN along with its low bioavailability might be responsible for low activation efficiency of the responsible signaling pathways for cell proliferation once the drug releases rapidly in the environment. Consequently, the linear release profile of KGN in the most controlled manner from the nanocomposite resulted in the highest cell proliferation.

Other than KGN, TGFβ1 is one of the famous growth factors being exploited in cartilage tissue engineering as it significantly boosts chondrogenesis of MSCs and induces lubricin accumulation to protect

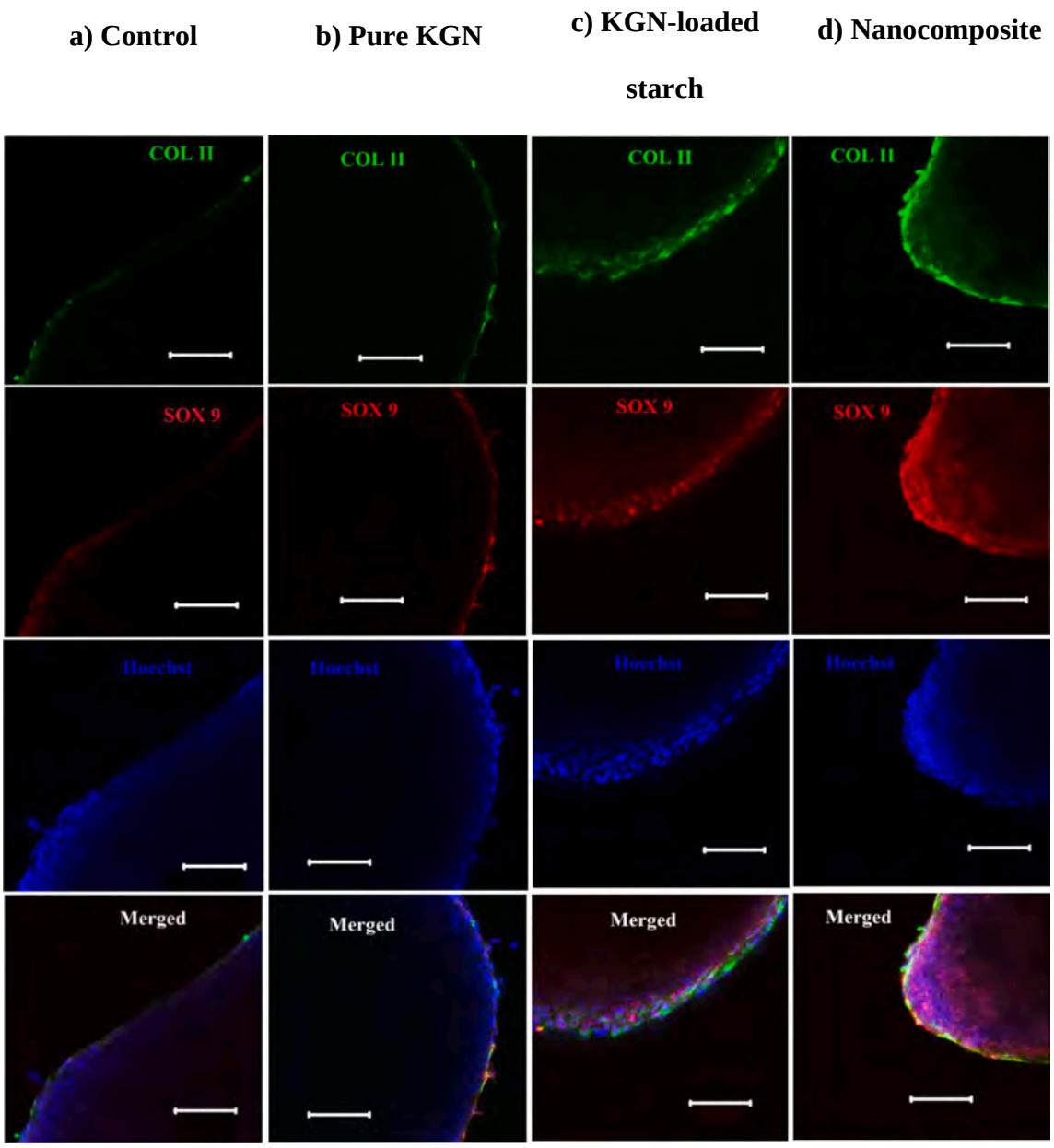

Fig. 8. Confocal laser scanning microscopy images of collagen type II (COL II), SOX9 and Hoechst staining of cell pellet sections: (a) Untreated control and samples treated with (b) pure KGN, (c) KGN-loaded starch microspheres and (d) Nanocomposite thermogel for 14 days (Scale bar: 100 μm).

cartilage [60]. Generally speaking, growth factors cause immunogenic reactions and have limited stability and short half-lives when used *in vivo* which hamper their applications. Consequently, small biomolecules like KGN have attracted scientists' attention since they are cheaper, stable, and small enough to bypass immune responses with little risk of cross-species contamination. Not only KGN elevates the chondrogenic differentiation of MSCs by regulating the CBFb-RUNX1 transcriptional programme, but also it has chondroprotective impacts on chondrocytes experiencing pathological situations while protecting the cartilage ECM from damage [58,60]. To compare the chondro-inductive effect of KGN with TGFβ1, Decker et al. [59] treated limb-bud mesenchymal cells for 24 h with 100 nM KGN or 2.5 ng/mL recombinant human TGFβ1. Results indicated that, these factors had quite similar chondrogenic effects in terms of GAG deposition and expression of TGFβ1, SOX9, MSX2 and TGFBI. Indeed, both stimulated overlapping downstream pathways such as Smad2/3 phosphorylation, hedgehog signaling, and SOX9 expression. Exposure of MSCs to TGFβ1 resulted in enhancing Smad1/5/8 (BMP Smads) phosphorylation other than Smad2/3 (TGFβ Smads). Such process led to upregulation of RUNX2 and consequently chondrocyte hypertrophy. On the contrary, KGN elevated Smad2/3 phosphorylation without any considerable impact on Smad1/5/8 phosphorylation which limits chondrocyte hypertrophy. Accordingly, KGN possesses a significant chondroprotective property [59].

The immunofluorescence images in Fig. 8 confirm increase in the expression of SOX9 (red) and COL II (green) when hAMSCs are treated with the KGN-containing samples compared to the control. Although the expression of these proteins by the cells exposed to KGN-loaded microspheres increases compared to pure KGN, the nanocomposite hydrogel produces the most prominent chondrogenic differentiation of hAMSCs due to the ability to deliver KGN in a more prolonged and regulated manner. Considering that MSCs in an osteoarthritic synovial fluid are beneficial targets in regenerative tissue engineering, our nanocomposite offers a potential injectable acellular "off-the-shelf" solution for cartilage regeneration [28]. Not only does extended, linear KGN release trigger chondrogenesis of MSCs in the osteoarthritic synovial fluid, but also prolonged DS release could modulate joint inflammation while the favorable shear-resistance properties can mechanically support cartilage defects. Despite of the promising *in vitro* results, further *in vivo* evaluations are needed to verify its potential clinical application.

4. Conclusion

A nanocomposite thermogel based on chitosan with unique properties is designed and demonstrated. This injectable scaffold possesses an exceptional shear modulus in addition to dual pro-chondrogenic and anti-inflammatory functions, rendering it suitable for cartilage tissue engineering. To produce better mechanical properties, HNTs are utilized as reinforcements in the chemically-modified chitosan hydrogel. KGN and DS are employed as therapeutics to stimulate chondrogenesis and suppress inflammation at the injured site, respectively. To accomplish prolonged drug release, KGN is encapsulated in the monodispersed starch microspheres by a droplet microfluidic chip and DS is loaded into the inner lumens of the HNTs. Drug carriers are then embedded into the gel to achieve extended and continuous dual drug release to improve the therapeutic efficacy and obviate the need for multiple injections. The nanocomposite hydrogel has an outstanding shear modulus of 167 ± 5 kPa that is comparable to that of native articular cartilage and a suitable gelation time of 5 ± 0.5 min at 37 °C boding well for clinical implementation. Improved chondrogenesis of hAMSCs is achieved when KGN is encapsulated in the starch microspheres compared to pure KGN and the nanocomposite thermogel is most effective in inducing chondrodifferentiation of hAMSCs. Based on the superior rheological properties, thermo-responsiveness, and long-term release of biological cues for chondrogenesis and pain reduction, this unique nanocomposite offers a feasible injectable acellular "off-the-shelf" solution for cartilage restoration.

CRediT authorship contribution statement

Dorsa Dehghan-Baniani: Conceptualization, Methodology, Validation, Formal analysis, Investigation, Writing – original draft, Writing – review & editing. **Babak Mehrjou:** Formal analysis, Investigation, Writing – review & editing. **Dong Wang:** Investigation. **Reza Bagheri:** Supervision, Writing – review & editing. **Atefeh Solouk:** Supervision, Writing – review & editing. **Paul K. Chu:** Supervision, Writing – review & editing, Funding acquisition. **Hongkai Wu:** Supervision, Writing – review & editing, Project administration, Funding acquisition.

Declaration of competing interest

The authors declare no conflict of interest.

Acknowledgments

The authors acknowledge funding from Research Grants Council (RGC, UGC) of Hong Kong through General Research Funds (GRF16308818 and GRF16309920 and GRF16309421), Hong Kong ITC (MHP/003/19) as well as City University of Hong Kong Strategic Research Grant (SRG) No. 7005264.

Appendix A. Supplementary data

Supplementary data to this article can be found online at https://doi.org/10.1016/j.ijbiomac.2022.02.115.

References

[1] A.C. Hall, The role of chondrocyte morphology and volume in controlling phenotype—implications for osteoarthritis, cartilage repair, and cartilage engineering, Curr. Rheumatol. Rep. 21 (2019) 38, https://doi.org/10.1007/s11926-019-0837-6.
[2] K. Goodarzi, F. Jonidi Shariatzadeh, A. Solouk, S. Akbari, H. Mirzadeh, Injectable drug loaded gelatin based scaffolds as minimally invasive approach for drug delivery system: CNC/PAMAM nanoparticles, Eur. Polym. J. 139 (2020), 109992, https://doi.org/10.1016/j.eurpolymj.2020.109992.
[3] F. Jonidi Shariatzadeh, A. Solouk, S. Bagheri Khoulenjani, S. Bonakdar, H. Mirzadeh, Injectable and reversible preformed cryogels based on chemically crosslinked gelatin methacrylate (GelMA) and physically crosslinked hyaluronic acid (HA) for soft tissue engineering, Colloids Surf. B: Biointerfaces 203 (2021), 111725, https://doi.org/10.1016/j.colsurfb.2021.111725.
[4] W. Wei, Y. Ma, X. Yao, W. Zhou, X. Wang, C. Li, J. Lin, Q. He, S. Leptihn, H. Ouyang, Advanced hydrogels for the repair of cartilage defects and regeneration, Bioact. Mater. 6 (2021) 998–1011, https://doi.org/10.1016/j.bioactmat.2020.09.030.
[5] J. Clouet, C. Vinatier, C. Merceron, M. Pot-vaucel, Y. Maugars, P. Weiss, G. Grimandi, J. Guicheux, From osteoarthritis treatments to future regenerative therapies for cartilage, Drug Discov. Today 14 (2009) 913–925, https://doi.org/10.1016/j.drudis.2009.07.012.
[6] A.I. Journal, A. Rahmani, D. Bakhshayesh, S. Babaie, H.T. Nasrabadi, N. Asadi, A. Akbarzadeh, A. Abedelahi, An overview of various treatment strategies, especially tissue engineering for damaged articular cartilage, Artif. Cells Nanomed. Biotechnol. 48 (2020) 1089–1104, https://doi.org/10.1080/21691401.2020.1809439.
[7] D. Dehghan-Baniani, B. Mehrjou, P.K. Chu, H. Wu, A biomimetic nano-engineered platform for functional tissue engineering of cartilage superficial zone, Adv. Healthc. Mater. 10 (2021) 2001018, https://doi.org/10.1002/adhm.202001018.
[8] P. Baei, H. Daemi, F. Mostafaei, F. Azam, A tough polysaccharide-based cell-laden double-network hydrogel promotes articular cartilage tissue regeneration in rabbits, Chem. Eng. J. 418 (2021), 129277.
[9] D. Dehghan Baniani, R. Bagheri, A. Solouk, Preparation and characterization of a composite biomaterial including starch micro/nano particles loaded chitosan gel, Carbohydr. Polym. 174 (2017) 633–645, https://doi.org/10.1016/j.carbpol.2017.06.095.
[10] D. Dehghan-Baniani, Y. Chen, D. Wang, R. Bagheri, A. Solouk, H. Wu, Injectable in situ forming kartogenin-loaded chitosan hydrogel with tunable rheological properties for cartilage tissue engineering, Colloids Surf. B: Biointerfaces 192 (2020), 111059, https://doi.org/10.1016/j.colsurfb.2020.111059.
[11] R. Yendluri, Y. Lvov, M.M. de Villiers, V. Vinokurov, E. Naumenko, E. Tarasova, R. Fakhrullin, Paclitaxel encapsulated in halloysite clay nanotubes for intestinal and intracellular delivery, J. Pharm. Sci. 106 (2017) 3131–3139, https://doi.org/10.1016/j.xphs.2017.05.034.
[12] W. Li, D. Liu, H. Zhang, A. Correia, E. Mäkilä, J. Salonen, J. Hirvonen, H.A. Santos, Microfluidic assembly of a nano-in-micro dual drug delivery platform composed of

halloysite nanotubes and a pH-responsive polymer for colon cancer therapy, Acta Biomater. 48 (2017) 238–246, https://doi.org/10.1016/j.actbio.2016.10.042.
[13] M.L. Kang, J.Y. Ko, J.E. Kim, G. il Im, Intra-articular delivery of kartogenin-conjugated chitosan nano/microparticles for cartilage regeneration, Biomaterials 35 (2014) 9984–9994, https://doi.org/10.1016/j.biomaterials.2014.08.042.
[14] J. Zhang, J.H.C. Wang, Kartogenin induces cartilage-like tissue formation in tendon-bone junction, Bone Res. 2 (2014) 12–17, https://doi.org/10.1038/boneres.2014.8.
[15] D. Dehghan-Baniani, P. Zahedifar, R. Bagheri, A. Solouk, Curcumin-loaded starch micro/nano particles for biomedical application: the effects of preparation parameters on release profile, Starch/Starke 71 (2019) 1800305, https://doi.org/10.1002/star.201800305.
[16] Q. Xu, M. Hashimoto, T.T. Dang, T. Hoare, D.S. Kohane, G.M. Whitesides, R. Langer, D.G. Anderson, H. David, Preparation of monodisperse biodegradable polymer microparticles using a microfluidic flow-focusing device for controlled drug delivery, Small 5 (2009) 1575–1581, https://doi.org/10.1002/smll.200801855.
[17] L. Rodrigues, M. Mota, Bioinspired Materials for Medical Applications, Woodhead Publishing, 2016.
[18] R. Tan, X. Niu, S. Gan, Q. Feng, Preparation and characterization of an injectable composite, J. Mater. Sci. Mater. Med. 20 (2009) 1245–1253.
[19] Y. Chen, F. Zhang, Q. Fu, Y. Liu, Z. Wang, N. Qi, In vitro proliferation and osteogenic differentiation of human dental pulp stem cells in injectable thermo-sensitive chitosan/b-glycerophosphate/hydroxyapatite hydrogel, J. Biomater. Appl. 31 (2016) 317–327, https://doi.org/10.1177/0885328216661566.
[20] B.G. Ballios, M.J. Cooke, D. van der Kooy, M.S. Shoichet, A hydrogel-based stem cell delivery system to treat retinal degenerative diseases, Biomaterials 31 (2010) 2555–2564, https://doi.org/10.1016/j.biomaterials.2009.12.004.
[21] M. Kang, J. Kim, G. Im, Thermoresponsive nanospheres with independent dual drug release profiles for the treatment of osteoarthritis, Acta Biomater. 39 (2016) 65–78, https://doi.org/10.1016/j.actbio.2016.05.005.
[22] N. Asgari, F. Bagheri, M.B. Eslaminejad, M.H. Ghanian, F.A. Sayahpour, A. M. Ghafari, Dual functional construct containing kartogenin releasing microtissues and curcumin for cartilage regeneration, Stem Cell Res Ther 11 (2020) 289, https://doi.org/10.1186/s13287-020-01797-2.
[23] S.S. Lee, G.E. Choi, H.J. Lee, Y. Kim, J.-H. Choy, B. Jeong, Layered double hydroxide and polypeptide thermogel nanocomposite system for chondrogenic differentiation of stem cells, ACS Appl. Mater. Interfaces 9 (2017) 42668–42675, https://doi.org/10.1021/acsami.7b17173.
[24] D. Shi, X. Xu, Y. Ye, K. Song, Y. Cheng, J. Di, Q. Hu, J. Li, H. Ju, Q. Jiang, Z. Gu, Photo-cross-linked scaffold with kartogenin-encapsulated nanoparticles for cartilage regeneration, ACS Nano 10 (2016) 1292–1299, https://doi.org/10.1021/acsnano.5b06663.
[25] Y. Lvov, W. Wang, L. Zhang, R. Fakhrullin, Halloysite clay nanotubes for loading and sustained release of functional compounds, Adv. Mater. 28 (2016) 1227–1250, https://doi.org/10.1002/adma.201502341.
[26] Y. Chen, L. Huang, X. Dai, Q. Tian, M. Yu, M. Agheb, H.N. Chan, E. Poon, Z. Guo, K. R. Boheler, H. Wu, Facile formation of a microporous chitosan hydrogel based on self-crosslinking, J. Mater. Chem. B 5 (2017) 9291–9299, https://doi.org/10.1039/c7tb02736b.
[27] A.J. DeMello, Control and detection of chemical reactions in microfluidic systems, Nature 442 (2006) 394–402, https://doi.org/10.1038/nature05062.
[28] S. Chen, H. Zhang, X. Shi, H. Wu, N. Hanagata, Microfluidic generation of chitosan/CpG oligodeoxynucleotide nanoparticles with enhanced cellular uptake and immunostimulatory properties, Lab Chip 14 (2014) 1842–1849, https://doi.org/10.1039/c4lc00015c.
[29] Z. Nie, M.S. Seo, S. Xu, P.C. Lewis, M. Mok, E. Kumacheva, G.M. Whitesides, P. Garstecki, H.A. Stone, Emulsification in a microfluidic flow-focusing device: effect of the viscosities of the liquids, Microfluid. Nanofluid. 5 (2008) 585–594, https://doi.org/10.1007/s10404-008-0271-y.
[30] I. Cumpstey, Chemical modification of polysaccharides, ISRN Org. Chem. 2013 (2013), 417672.
[31] Đ. Ačkar, D. Šubarić, J. Babić, B. Miličević, A. Jozinović, Modification of wheat starch with succinic acid/acetanhydride and azelaic acid/acetanhydride mixtures. II. Chemical and physical properties, J. Food Sci. Technol. 51 (2014) 1463–1472, https://doi.org/10.1007/s13197-012-0642-y.
[32] D. Demirgöz, C. Elvira, J.F. Mano, A.M. Cunha, E. Piskin, R.L. Reis, Chemical modification of starch based biodegradable polymeric blends: effects on water uptake, degradation behaviour and mechanical properties, Polym. Degrad. Stab. 70 (2000) 161–170, https://doi.org/10.1016/S0141-3910(00)00102-6.
[33] K. Krejčová, P.B. Deasy, M. Rabišková, Diclofenac sodium entrapment and release from halloysite nanotubules, Ces. Slov. 62 (2013) 28–34.
[34] I. Pountos, P.V. Giannoudis, E. Jones, A. English, S. Churchman, S. Field, F. Ponchel, H. Bird, P. Emery, D. Mcgonagle, NSAIDS inhibit in vitro MSC chondrogenesis but not osteogenesis: implications for mechanism of bone formation inhibition in man, J. Cell. Mol. Med. 15 (2011) 525–534, https://doi.org/10.1111/j.1582-4934.2010.01006.x.
[35] E.A. Naumenko, I.D. Guryanov, R. Yendluri, Y.M. Lvov, R.F. Fakhrullin, Clay nanotube-biopolymer composite scaffolds for tissue engineering, Nanoscale 8 (2016) 7257–7271, https://doi.org/10.1039/c6nr00641h.
[36] E. Abdullayev, Y. Lvov, Halloysite clay nanotubes as a ceramic "skeleton" for functional biopolymer composites with sustained drug release, J. Mater. Chem. B 1 (2013) 2894–2903, https://doi.org/10.1039/c3tb20059k.
[37] H. Liu, Z. Wang, X. Yao, Y. Chen, S. Shen, Intracellular pathway of halloysite nanotubes: potential application for antitumor drug delivery, J. Mater. Sci. 54 (2019) 693–704, https://doi.org/10.1007/s10853-018-2775-5.
[38] G. Fletes-vargas, H. Espinosa-andrews, M.L. Pita-l, Physically cross-linked chitosan-based hydrogels for tissue engineering applications: a state-of-the-art review, Eur. Polym. J. 145 (2021), 110176, https://doi.org/10.1016/j.eurpolymj.2020.110176.
[39] M.R. Buckley, J.P. Gleghorn, L.J. Bonassar, I. Cohen, Mapping the depth dependence of shear properties in articular cartilage, J. Biomech. 41 (2008) 2430–2437, https://doi.org/10.1016/j.jbiomech.2008.05.021.
[40] M. Mousa, N.D. Evans, R.O.C. Oreffo, J.I. Dawson, Clay nanoparticles for regenerative medicine and biomaterial design: a review of clay bioactivity, Biomaterials. 159 (2018) 204–214, https://doi.org/10.1016/j.biomaterials.2017.12.024.
[41] M. Liu, C. Wu, Y. Jiao, S. Xiong, C. Zhou, Chitosan-halloysite nanotubes nanocomposite scaffolds for tissue engineering, J. Mater. Chem. B 1 (2013) 2078–2089, https://doi.org/10.1039/c3tb20084a.
[42] D. Su, L. Jiang, X. Chen, J. Dong, Z. Shao, Enhancing the gelation and bioactivity of injectable silk fibroin hydrogel with laponite nanoplatelets, ACS Appl. Mater. Interfaces 8 (2016) 9619–9628, https://doi.org/10.1021/acsami.6b00891.
[43] M. Liu, Y. Zhang, C. Wu, S. Xiong, C. Zhou, Chitosan/halloysite nanotubes bionanocomposites: structure, mechanical properties and biocompatibility, Int. J. Biol. Macromol. 51 (2012) 566–575, https://doi.org/10.1016/j.ijbiomac.2012.06.022.
[44] D. Dehghan-Baniani, S.A.J. Jahromi, S.M. Zebarjad, A study on role of nanosized SiO 2 on deformation mechanism of vinyl ester, Bull. Mater. Sci. 37 (2014) 1677–1683.
[45] H. Wu, S. Wang, H. Fang, X. Zan, J. Zhang, Y. Wan, Chitosan-polycaprolactone copolymer microspheres for transforming growth factor-β1 delivery, Colloids Surf. B: Biointerfaces 82 (2011) 602–608, https://doi.org/10.1016/j.colsurfb.2010.10.024.
[46] G. Filardo, E. Kon, F. Perdisa, B. di Matteo, A. di Martino, F. Iacono, S. Zaffagnini, F. Balboni, V. Vaccari, M. Marcacci, Osteochondral scaffold reconstruction for complex knee lesions: a comparative evaluation, Knee 20 (2013) 570–576, https://doi.org/10.1016/j.knee.2013.05.007.
[47] A.B. Houreh, E. Masaeli, M.H. Nasr-esfahani, Chitosan/polycaprolactone multilayer hydrogel: a sustained Kartogenin delivery model for cartilage regeneration, Int. J. Biol. Macromol. 177 (2021) 589–600, https://doi.org/10.1016/j.ijbiomac.2021.02.122.
[48] X. Sun, J. Wang, Y. Wang, Q. Zhang, Collagen-based porous scaffolds containing PLGA microspheres for controlled kartogenin release in cartilage tissue engineering, Artif. Cells Nanomed. Biotechnol. 46 (2018) 1957–1966, https://doi.org/10.1080/21691401.2017.1397000.
[49] Y. Zhu, J. Tan, H. Zhu, G. Lin, F. Yin, L. Wang, K. Song, Y. Wang, G. Zhou, W. Yi, Development of kartogenin-conjugated chitosan-hyaluronic acid hydrogel for nucleus pulposus regeneration, Biomater. Sci. 5 (2017) 784–791, https://doi.org/10.1039/c7bm00001d.
[50] M. Iftime, L. Mititelu, L. Marin, New formulations based on salicyl-imine-chitosan hydrogels for prolonged drug release, Int. J. Biol. Macromol. 160 (2020) 398–408, https://doi.org/10.1016/j.ijbiomac.2020.05.207.
[51] L. Lisuzzo, G. Cavallaro, S. Milioto, G. Lazzara, Halloysite nanotubes filled with salicylic acid and sodium diclofenac: effects of vacuum pumping on loading and release properties, J. Nanostruct. Chem. 11 (2021) 663–673, https://doi.org/10.1007/s40097-021-00391-z.
[52] A.J. Sophia Fox, A. Bedi, S.A. Rodeo, The basic science of articular cartilage: structure, composition, and function, Sports Health 1 (2009) 461–468, https://doi.org/10.1177/1941738109350438.
[53] J. Varshosaz, Z.S. Sajadi-Javan, M. Kouhi, M. Mirian, Effect of bassorin (derived from gum tragacanth) and halloysite nanotubes on physicochemical properties and the osteoconductivity of methylcellulose-based injectable hydrogels, Int. J. Biol. Macromol. 192 (2021) 869–882, https://doi.org/10.1016/j.ijbiomac.2021.10.009.
[54] A. Kumar, S.M. Zo, J.H. Kim, S.C. Kim, S.S. Han, Enhanced physical, mechanical, and cytocompatibility behavior of polyelectrolyte complex hydrogels by reinforcing halloysite nanotubes and graphene oxide, Compos. Sci. Technol. 175 (2019) 35–45, https://doi.org/10.1016/j.compscitech.2019.03.008.
[55] R. Jin, L.S.M. Teixeira, P.J. Dijkstra, M. Karperien, C.A. van Blitterswijk, Z. Y. Zhong, J. Feijen, Injectable chitosan-based hydrogels for cartilage tissue engineering, Biomaterials 30 (2009) 2544–2551, https://doi.org/10.1016/j.biomaterials.2009.01.020.
[56] H. Sá-Lima, S.G. Caridade, J.F. Mano, R.L. Reis, Stimuli-responsive chitosan-starch injectable hydrogels combined with encapsulated adipose-derived stromal cells for articular cartilage regeneration, Soft Matter 6 (2010) 5184, https://doi.org/10.1039/c0sm00041h.
[57] H. Jing, X. Zhang, M. Gao, K. Luo, W. Fu, M. Yin, W. Wang, Z. Zhu, Kartogenin preconditioning commits mesenchymal stem cells to a precartilaginous stage with enhanced chondrogenic potential by modulating JNK and b-catenin 2 related pathways, FASEB J. 33 (2019) 5641–5653, https://doi.org/10.1096/fj.201802137RRR.
[58] T. Liu, X. Li, T. Wang, X. Chen, S. Zhang, J. Liao, W. Wang, X. Zou, G. Zhou, Kartogenin mediates cartilage regeneration by stimulating the IL-6/Stat3-dependent proliferation of cartilage stem/progenitor cells, Biochem. Biophys. Res. Commun. 532 (2020) 385–392, https://doi.org/10.1016/j.bbrc.2020.08.059.
[59] R.S. Decker, E. Koyama, M. Enomoto-Iwamoto, P. Maye, D. Rowe, S. Zhu, P. G. Schultz, M. Pacifici, Mouse limb skeletal growth and synovial joint development are coordinately enhanced by Kartogenin, Dev. Biol. 395 (2014) 255–267, https://doi.org/10.1016/j.ydbio.2014.09.011.
[60] G. Cai, W. Liu, Y. He, J. Huang, L. Duan, J. Xiong, L. Liu, D. Wang, Recent advances in kartogenin for cartilage regeneration, J. Drug Target. 27 (2019) 28–32, https://doi.org/10.1080/1061186X.2018.1464011.

Supporting Information

A dual functional chondro-inductive chitosan thermogel with high shear modulus and sustained drug release for cartilage tissue engineering

Dorsa Dehghan-Baniani[a,b], Babak Mehrjou[c], Dong Wang[d], Reza Bagheri[b], Atefeh Solouk[e] , Paul K. Chu[c] and Hongkai Wu[a,d,*]

[a] Department of Chemical and Biological Engineering, Division of Biomedical Engineering, The Hong Kong University of Science and Technology, Hong Kong, China

[b] Polymeric Materials Research Group, Department of Materials Science and Engineering, Sharif University of Technology, Tehran, P.O. Box 11155-9466, Iran

[c] Department of Physics, Department of Materials Science and Engineering, and Department of Biomedical Engineering, City University of Hong Kong, Tat Chee Avenue, Kowloon, Hong Kong, China

[d] Department of Chemistry, The Hong Kong University of Science and Technology, Hong Kong, China (H.K. Wu: chhkwu@ust.hk)

[e] Department of Biomedical Engineering, Amirkabir University of Technology, Tehran, Iran

1. Cytocompatibility assays on drug-loaded particles

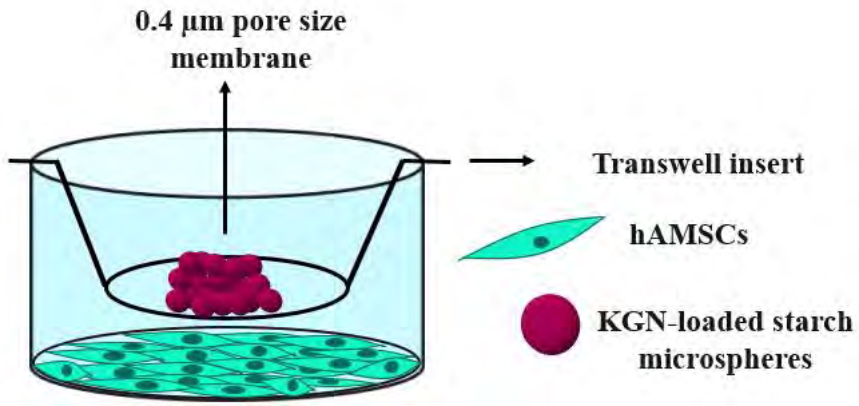

Figure S1. Schematic illustration of the cytocompatibility assays using transwell inserts with 0.4-μm pore size membrane.

2. Immunofluorescence staining

The cell pellets untreated or treated with pure KGN, KGN-loaded starch microspheres, and nanocomposite thermogel were assessed by immunofluorescence staining after cell culturing for 14 days. The primary antibodies in the experiments included anti-collagen-II (Cat. No. ab185430) and anti-SOX9 antibodies (Cat. No. ab185966) obtained from Abcam. The cell pellets were washed with PBS and incubated with paraformaldehyde (4 wt.%) for 15 min. After fixation, the samples were washed with PBS and permeabilized with Triton X-100 (0.1% in PBS) for 45 min (at 25 ºC). The cell pellets were washed again and incubated with 1 wt.% bovine serum albumin (in PBS) for 1 h at 25 ºC to

minimize non-specific binding of the primary antibodies in the cells. Subsequently, the samples were incubated with primary antibodies of SOX9 (5 µg/ml) and collagen-II (2 µg/ml) at 4 ºC overnight. After washing the cell pellets with PBS, Goat Anti-Rabbit IgG (Alexa Flour 594, Invitrogen, Cat. No. A-11012) and Goat Anti-Mouse IgG (Alexa Flour 488, Invitrogen, Cat. No. A32723) as the secondary antibodies were added to the samples and kept at 25 ºC for 2 h. The concentration of the secondary antibodies was adjusted to 2 µg/ml. The pellets were washed with PBS three times and treated with Hoechst at room temperature. Finally, immunofluorescence staining was performed and observation was made under a confocal laser scanning microscope (CLSM, TCS SP5 II, Leica).

3. DNA and GAG contents

After cell culturing for 21 days, the contents of DNA and sulfated glycosaminoglycan (s-GAG) in the cell pellets were determined. A papain solution (25 µg/ml in 50 mM sodium phosphate, 2 mM EDTA, and 2mM N-acetyl cysteine pH 6.5) was utilized as the digesting reagent. 1 ml of the digesting solution was added to each cell pellet and incubated at 65 ºC overnight. The DNA amount of each digest was determined by a Quant-iT PicoGreen dsDNA assay kit (Cat. No. p11496) according to the manufacturer's protocol. Fluorescence from the samples was recorded by a fluorescence microplate reader (excitation ~ 480 nm, emission ~ 520 nm). To quantify the s-GAG content in the digests, a Blyscan kit (Biocolor, Carrickfergus, UK) was used according to the manufacturer's suggested protocol. The kit technique was based on specific binding of the proteoglycans s-GAG chains and protein-free s-GAG chains to a cationic dye (1,9-DMMB). The dye reagent was mixed with the digests for 30 min to generate the s-GAG-dye complex. In the next step, the samples were centrifuged at 12,000 rpm for 10 min and

the supernatants were discarded from the created complexes. The s-GAG-dye complexes collected were blended with a dissociation buffer for 10 min and the absorbance of the released dye was measured at 656 nm by a microplate reader. Bovine tracheal chondroitin 4-sulfate was utilized to draw standard curves for the quantitative analysis. The experiments were repeated three times for each set of conditions [1–4].

4. qRT-PCR analysis

The gene expression levels were studied with a one-step qRT-PCR kit using the following protocol:

1. cDNA synthesis at 50 ºC for 3 min,

2. Denaturation at 95 ºC for 5 min,

3. Amplification (45 cycles at 95 ºC for 15 s and 60 ºC for 30 s),

4. Melting (95 ºC for 5 s, 65 ºC for 1 min and 0.11 ºC/s to 97 ºC),

5. Cooling (40 ºC for 30 s).

The primer sequences used in the experiments are presented in Table S1.

Table S1. Primer sequences used in qRT-PCR experiments

Gene symbol	**Forward primer ($5' - 3'$)**	**Reverse primer ($5' - 3'$)**
COL2A1	AACCAGATTGAGAGCATCCG	ACCTTCATGGCGTCCAAG
COL1A1	CCCCTGGAAAGAATGGAGATG	TCCAAACCACTGAAACCTCTG
COL10A1	CAGTCATGCCTGAGGGTTTT	GGGTCATAATGCTGTTGCCT
Aggrecan	TCGAGGACAGCGAGGCC	TCGAGGGTGTAGCGTGTAGAGA
SOX9	ACCTTTGGGCTGCCTTATATT	TCCCTCACTCCAAGAGAAGAT

GAPDH	CACATGGCCTCCAAGGAGTAA	GTACATGACAAGGTGCGGCTC

5. X-ray diffraction

X-ray diffraction (XRD) was conducted on TSTMP, pure starch and crosslinked starch microspheres on the Philips PW1830 at 40 kV and 30 mA with copper tube (wavelength 1.54060 Å) radiation. The samples were scanned from 5° to 40° (2θ) with a scanning speed of 0.25 min^{-1} and sampling interval of 0.02° [5]. The XRD patterns of pure starch, pure TSTMP and crosslinked starch microspheres are displayed in Figure S2. Figure S2a shows that the crosslinker (TSTMP) has a highly crystalline structure as reflected by the strong peaks between 2θ = 10° and 40°. There are several sharp peaks at 2θ = 6°, 15°, 17°, 23°, 24° and 38° indicating the existence of some crystalline regions in the pure starch sample (Figure S2b). However, the XRD pattern of the crosslinked starch microspheres is smooth showing a broad peak at 2θ = 20° (Figure S2c), implying that the microspheres have a mainly amorphous structure with limited crystallinity. These mentioned peaks from pure starch and TSTMP cannot be observed from the crosslinked microspheres, indicating that starch is successfully crosslinked and no TSTMP with a crystalline structure remains in the crosslinked microspheres. These results are consistent with results reported previously on the preparation of starch particles [5,6].

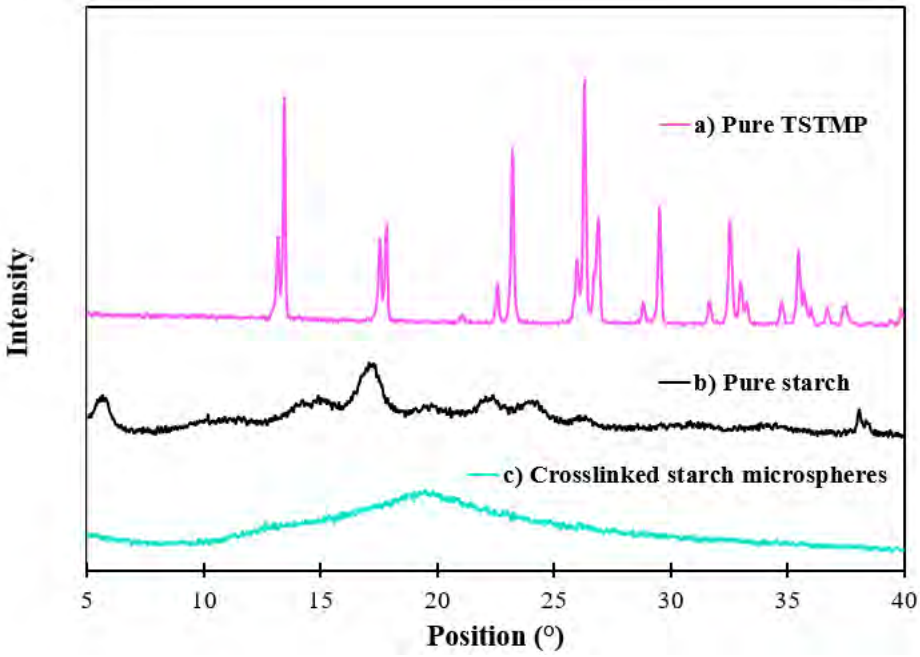

Figure S2. XRD patterns of (a) Pure TSTMP, (b) Pure starch and (c) Crosslinked starch microspheres.

6. Swelling measurements

6.1. Swelling studies of starch microspheres

In order to investigate the swelling behavior of the starch microspheres, 30 mg (W_0) of the starch microspheres (bare or loaded with KGN) were soaked in 2 ml of PBS at 37 ºC. At the designated time points, the excess PBS was removed and the weight of the swollen particles was determined (W_{sw}). The swelling percentage was calculated by the following equation:[7]

$$Swelling\ percentage = \frac{W_{sw} - W_0}{W_0} \times 100 \quad . \qquad (1)$$

The swelling percentages of the bare and KGN-loaded starch microspheres are given in Figure S3.

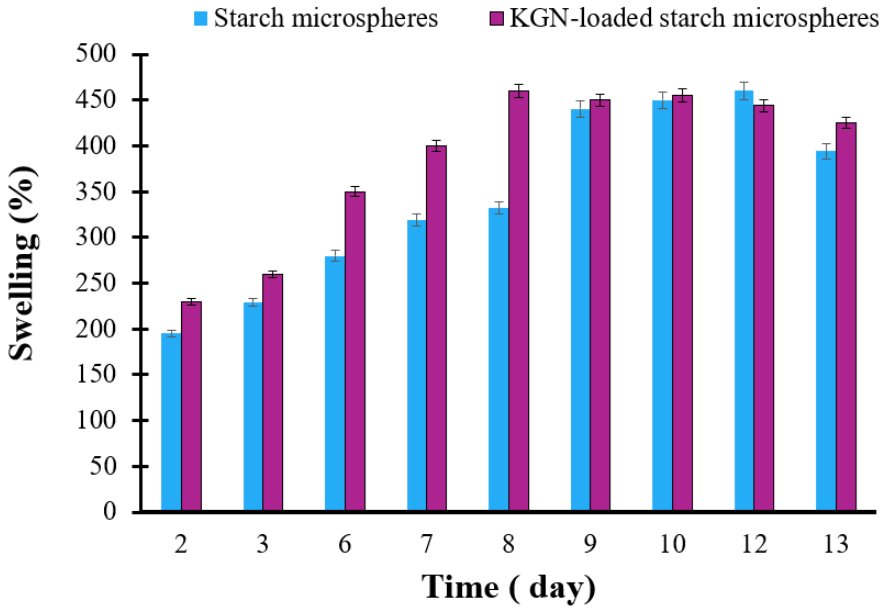

Figure S3. Swelling percentages of the bare and KGN-loaded starch microspheres.

6.2. Swelling studies of chitosan hydrogels

Hydrogels (~150 µl) made in 2-mL plastic tubes (Axygen®, Cat. No. MCT-200-C, Corning Life Sciences) were kept at 37 °C overnight to attain full mechanical stability. After measuring the initial weight (W_i), 1.5 ml of PBS were added to each tube and at the designated time points, PBS was discarded and the weight of the swollen gel was determined (W_s). After each measurement, fresh PBS was added to each sample until the last time point. The hydrogels swelling coefficients (Q) were estimated by the following equation:[5]

$$Swelling\ coefficient = \frac{W_s}{W_i} \quad . \qquad (2)$$

7. Attenuated Total Reflectance-Fourier Transform Infrared measurements

Attenuated total reflectance-Fourier transform infrared (ATR-FTIR) was performed on chitosan, BMPS-modified chitosan, pure KGN, pure starch, crosslinked starch microspheres, KGN-loaded starch microspheres, pure HNTs, pure DS and DS-loaded HNTs using a Bruker FTIR (Vertex 70 Hyperion 1000, USA). Each sample was examined in the wavenumber range of 400 – 4000 cm^{-1} and at 32 scans.

The ATR-FTIR spectra of pure HNTs, pure DS, and DS-loaded HNTs are shown in Figure 3a. The absorption peaks at 3694 cm^{-1} and 3622 cm^{-1} are related to O–H stretching vibration of Al–OH on the inner surface and inner Al–OH groups between the interface of the Al–O octahedron and the Si–O tetrahedron in HNTs, respectively. There are two other peaks at around 910 cm^{-1} and 1000 cm^{-1} which can be assigned to Si-O stretching and O-H deformation in the inner hydroxyl groups, respectively [8,9]. The peaks at 1280 cm^{-1} and 1300 cm^{-1} of DS are related to C-N stretching, whereas the DS peaks at 1507 cm^{-1} and 1579 cm^{-1} are assigned to C=C stretching and C=O stretching of the carboxyl groups, respectively. The distinct peak at around 3320 cm^{-1} corresponds to amino peak (NH-stretching) in DS [10,11]. In the FTIR spectra of the DS-loaded HNTs, various characteristic peaks of DS and HNTs can be distinguished without significant shifting, suggesting that there is no chemical interaction between DS and HNTs. In other words, the DS molecules are simply entrapped mechanically within the hollow nanotubes by means of the vacuum pump [12].

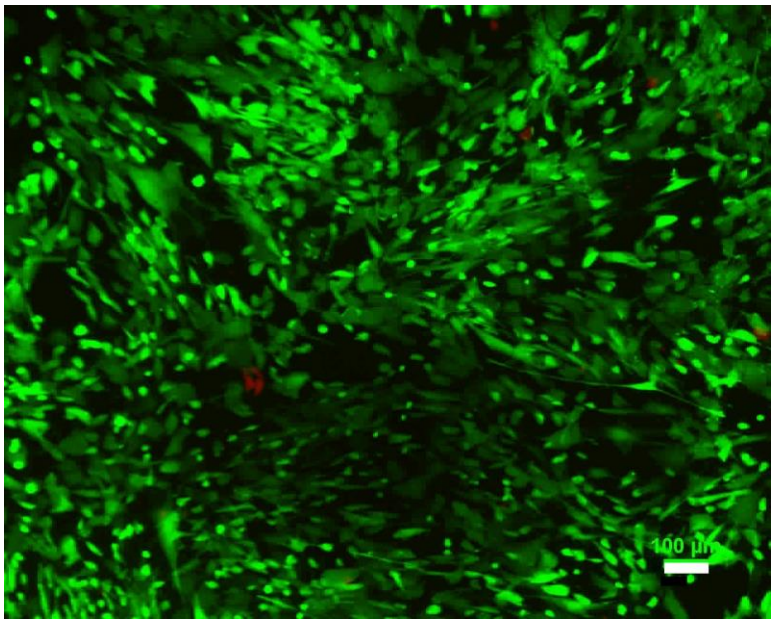

Figure S4. Cell viability of hAMSCs incubated with pure HNTs for 48 h (scale bar: 100 µm).

8. *In vitro* degradation

The hydrogel precursor solutions (~0.7 g) with different formulations including (a) chitosan hydrogel (sample No. 1), (b) hydrogel containing 6 w/v% HNTs (sample No. 4), and (c) nanocomposite thermogel (sample No. 6) were incubated at 37 ºC. The gel weights were determined (W_i) and 2 ml of PBS containing lysozyme (1 mg/mL) and α-amylase (150 U/L) were poured on the top of each sample and kept at 37 ºC. The solution was removed from the samples at certain time points and the weights were measured (W_t). By using Eq. 3 the weight percentages of the remaining gels were determined [1,13,14]. The degradation medium was changed two times per week and the experiments were repeated three times.

$$Remaining\ gel\ (wt.\%) = \frac{W_t}{W_i} \times 100 \quad . \qquad (3)$$

8.1.Enzymatic degradation evaluations

Both starch and chitosan degrade enzymatically *in vitro* and *in vivo* [1,13,14]. Degradation of chitosan occurs due to the enzymatic hydrolysis of glycosidic bonds of the acetylated residues in chitosan chains when they are exposed to lysozyme. About 0.5 to 2 mg/mL of this protein can be found from the human cartilage ECM. Moreover, starch undergoes enzymatic degradation in the presence of enzymes such as α-amylase which is also found in human fluids (150 U/L). Consequently, to mimic the physiological environment in the degradation experiments, PBS containing 150 U/L α-amylase and 1 mg/mL lysozyme was employed as the degradation solution [1,13,14]. On the other hand, HNTs are non-degradable at a neutral pH and 37 ºC [15], but as shown by previous *in vivo* tests [8], combination with degradable biomaterials such as chitosan and starch provides a suitable biodegradable platform. The hydrogel containing 6 w/v% HNTs (sample No. 4) exhibits a smaller degradation rate than the control (sample No. 1) [1]. Since HNTs act as physical crosslinkers, they increase the crosslinking density significantly and decrease the swelling and degradation rate. However, the nanocomposite thermogel (sample No. 6) shows faster degradation than the hydrogel containing only HNTs (sample No.4) due to the existence of the degradable starch particles in the structure [14]. The *in vitro* degradation trend of the nanocomposite thermogel (Figure S5) implies that it is not likely to be entirely degraded in one month and degradation occurs mainly through the surface [1].

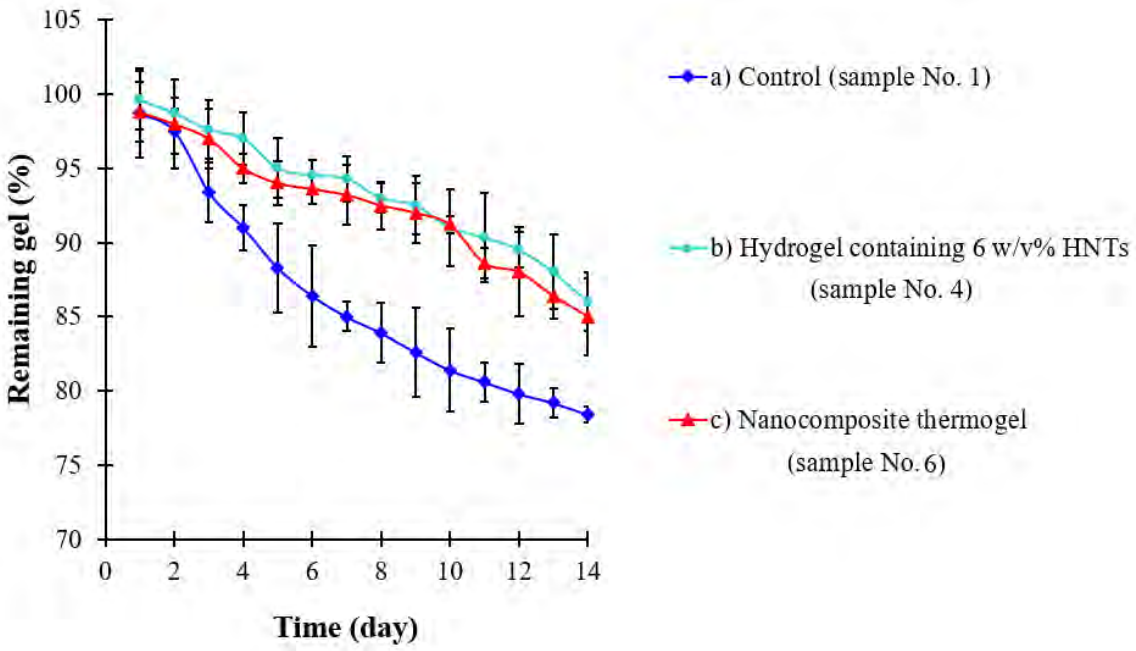

Figure S5. Enzymatic degradation trend of (a) Chitosan hydrogel [1] (control, sample No. 1), (b) Hydrogel containing 6 w/v% HNTs (sample No. 4), and (c) Nanocomposite thermogel (sample No. 6).

References:

[1] D. Dehghan-Baniani, Y. Chen, D. Wang, R. Bagheri, A. Solouk, H. Wu, Injectable in situ forming kartogenin-loaded chitosan hydrogel with tunable rheological properties for cartilage tissue engineering, Colloids Surf. B. 192 (2020) 111059. doi:10.1016/j.colsurfb.2020.111059.

[2] M.L. Kang, J.Y. Ko, J.E. Kim, G. Il Im, Intra-articular delivery of kartogenin-conjugated chitosan nano/microparticles for cartilage regeneration, Biomaterials. 35 (2014) 9984–9994. doi:10.1016/j.biomaterials.2014.08.042.

[3] S.S. Lee, G.E. Choi, H.J. Lee, Y. Kim, J.-H. Choy, B. Jeong, Layered double hydroxide and polypeptide thermogel nanocomposite system for chondrogenic differentiation of stem Cells, ACS Appl. Mater. Interfaces. 9 (2017) 42668–42675. doi:10.1021/acsami.7b17173.

[4] M.S. Ponticiello, R.M. Schinagl, S. Kadiyala, F.P. Barry, Gelatin-based resorbable sponge as a carrier matrix for human mesenchymal stem cells in cartilage regeneration therapy, J. Biomed. Mater. Res. 52 (2000) 246–255.

[5] D. Dehghan-Baniani, R. Bagheri, A. Solouk, Preparation and characterization of a composite biomaterial including starch micro / nano particles loaded chitosan gel, Carbohydr. Polym. 174 (2017) 633–645. doi:10.1016/j.carbpol.2017.06.095.

[6] B.Z. Li, L.J. Wang, D. Li, B. Adhikari, Z.H. Mao, Preparation and characterization of crosslinked starch microspheres using a two-stage water-in-water emulsion method, Carbohydr. Polym. 88 (2012) 912–916. doi:10.1016/j.carbpol.2012.01.043.

[7] S.G. Nanaki, G.Z. Kyzas, A. Tzereme, M. Papageorgiou, M. Kostoglou, D.N. Bikiaris, D.A. Lambropoulou, Synthesis and characterization of modified carrageenan microparticles for the removal of pharmaceuticals from aqueous solutions, Colloids Surf. B. 127 (2015) 256–265. doi:10.1016/j.colsurfb.2015.01.053.

[8] E.A. Naumenko, I.D. Guryanov, R. Yendluri, Y.M. Lvov, R.F. Fakhrullin, Clay nanotube-biopolymer composite scaffolds for tissue engineering, Nanoscale. 8 (2016) 7257–7271. doi:10.1039/c6nr00641h.

[9] M. Liu, C. Wu, Y. Jiao, S. Xiong, C. Zhou, Chitosan-halloysite nanotubes nanocomposite scaffolds for tissue engineering, J. Mater. Chem. B. 1 (2013) 2078–2089. doi:10.1039/c3tb20084a.

[10] G. Murtaza, M. Ahmad, G. Shahnaz, Microencapsulation of Diclofenac Sodium by Non- solvent Addition Technique, Pharm Res Trop. J. Pharm. Res. April Trop J Pharm Res. 9 (2010) 187–187. http://www.tjpr.org.

[11] A.K. Nayak, D. Pal, Development of pH-sensitive tamarind seed polysaccharide-alginate composite beads for controlled diclofenac sodium delivery using response surface methodology, Int. J. Biol. Macromol. 49 (2011) 784–793. doi:10.1016/j.ijbiomac.2011.07.013.

[12] K. Krejčová, P.B. Deasy, M. Rabišková, Diclofenac sodium entrapment and release from halloysite nanotubules, Ces. a Slov. Farm. 62 (2013) 28–34.

[13] R. Jin, L.S.M. Teixeira, P.J. Dijkstra, M. Karperien, C.A. Van Blitterswijk, Z.Y. Zhong, J. Feijen, Injectable chitosan-based hydrogels for cartilage tissue

engineering, Biomaterials. 30 (2009) 2544–2551. doi:10.1016/j.biomaterials.2009.01.020.

[14] H. Sá-Lima, S.G. Caridade, J.F. Mano, R.L. Reis, Stimuli-responsive chitosan-starch injectable hydrogels combined with encapsulated adipose-derived stromal cells for articular cartilage regeneration, Soft Matter. 6 (2010) 5184. doi:10.1039/c0sm00041h.

[15] E. Abdullayev, Y. Lvov, Halloysite clay nanotubes as a ceramic "skeleton" for functional biopolymer composites with sustained drug release, J. Mater. Chem. B. 1 (2013) 2894–2903. doi:10.1039/c3tb20059k.